COLLISION-INDUCED INFRARED ABSORPTION OF HYDROGEN IN H_2-He AND H_2-Ne MIXTURES AT DIFFERENT TEMPERATURES

KAI-SIUNG CHANG, B.SC.

13661

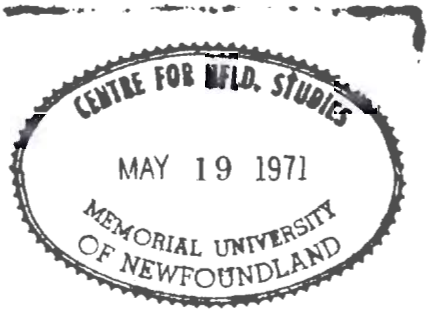
CENTRE FOR NFLD. STUDIES
MAY 19 1971
MEMORIAL UNIVERSITY
OF NEWFOUNDLAND

COLLISION-INDUCED INFRARED ABSORPTION OF HYDROGEN IN H_2-He AND H_2-Ne MIXTURES AT DIFFERENT TEMPERATURES

by

Kai-Siung Chang, B.Sc.

Submitted in partial fulfilment
of the requirements for the degree of Master of Science
Memorial University of Newfoundland

January, 1971

CONTENTS

ABSTRACT

The collision-induced fundamental infrared absorption band of hydrogen in H_2-He and H_2-Ne mixtures at 77^oK, 195^oK, 273^oK and 298^oK has been studied for gas densities up to 530 amagat for several base densities of hydrogen. In each of these mixtures the enhancement absorption profiles show, in addition to the usual splitting of the Q branch into the main Q_P and Q_R components, a splitting of the S(1) line into the $S_P(1)$ and $S_R(1)$ components at all the experimental temperatures, and a secondary splitting of the main Q_P component into the $Q_P(3)$ and $Q_R(3)$ components at 273^oK and 298^oK. The profiles of H_2-He at 77^oK also show a splitting of the S(0) line into $S_P(0)$ and $S_R(0)$. Integrated absorption coefficients were measured and binary and ternary absorption coefficients were derived. Van Kranendonk's theory of the 'exp-4' model for the induced dipole moment was applied to the experimental binary absorption coefficients. The quadrupolar parts of these coefficients were calculated from the known molecular parameters. These were then subtracted from the experimental values to obtain the overlap parts. The overlap parameters λ and ρ, giving respectively the magnitude and range of the overlap moment, were determined for each of the mixtures by obtaining the best fit of the calculated overlap part of the binary absorption coefficient as a function of temperature to the experimental values of the overlap parts. The values of λ and ρ are as follows:

Mixture	λ	ρ
H_2-He	5.6×10^{-3}	0.24Å
H_2-Ne	9.0×10^{-3}	0.29Å

CHAPTER 1

INTRODUCTION

It is well known that an isolated homonuclear diatomic molecule, such as hydrogen, has no dipole moment in any of its static, translational, rotational and vibrational states. Dipole absorption is therefore forbidden for such isolated molecular species at their translational and vibrational frequencies. However, an induced dipole moment can occur in a colliding pair of molecules because of an asymmetric distortion of their electron configuration. This induced dipole moment is modulated at the translational, rotational and vibrational frequencies of the molecules. Consequently, the colliding molecular pair can absorb energy from a radiation field at these frequencies. The collision-induced infrared absorption was first discovered by Crawford, Welsh and Locke (1949) who observed the fundamental vibration bands in liquid and compressed oxygen and in compressed nitrogen.

Since the discovery of collision-induced infrared absorption the induced fundamental band of gaseous hydrogen has been studied experimentally over a wide range of pressures and temperatures; some theoretical studies of the phenomenon have also been made. The reasons for the great amount of interest in the study of the spectrum of hydrogen are many: the hydrogen molecule is the simplest of all the diatomic molecules; it can be treated more rigorously by theoretical calculations; the rotational components of the band are widely separated because of the small moment of inertia of the molecule. The

fundamental band was studied in pure H_2 and in binary mixtures, H_2-He, H_2-Ar and H_2-N_2, at pressures up to 1500 atm in the temperature range 80^oK - 376^oK by Chisholm and Welsh (1954) and at pressures up to 5000 atm at room temperature by Hare and Welsh (1958). Subsequently, Hunt (1959) studied the induced absorption of the band in greater detail in pure H_2 in the temperature range 40^oK - 300^oK and in H_2-He in the temperature range 85^oK - 300^oK. Later, Watanabe and Welsh (1965) studied the band in pure H_2 at pressures of the order of 1 atm in the temperature range 18^oK - 77^oK and in H_2-He at 20^oK. More recently, in our laboratory, the band was studied at room temperature in H_2-Ne and H_2-Kr by Reddy and Lee (1968) and in H_2-O_2 and H_2-Xe by Varghese and Reddy (1969).

Condon (1932) showed that the dipole moment induced in a molecule by a static electric field gives rise to the forbidden transitions which obey the Raman rather than the infrared selection rules. In the absorption induced by intermolecular forces, the polarization of the absorbing molecule by a perturbing molecule would produce a similar effect. The collision-induced infrared absorption of the fundamental bands of homonuclear diatomic molecules was hence found to obey the Raman selection rules for rotation, i.e., $\Delta J = -2$ (O branch), 0 (Q branch), and +2 (S branch), where J is the rotational quantum number. For the fundamental absorption band of hydrogen ($v' = 1, J' \leftarrow v'' = 0, J''$), possible single transitions between the lower and upper rotational states at room temperature are illustrated in Fig. 1. Here the vibrational and rotational term values $G_0(v)$ and $F_v(J)$, respectively, were calculated using the molecular constants obtained by Stoicheff (1957).

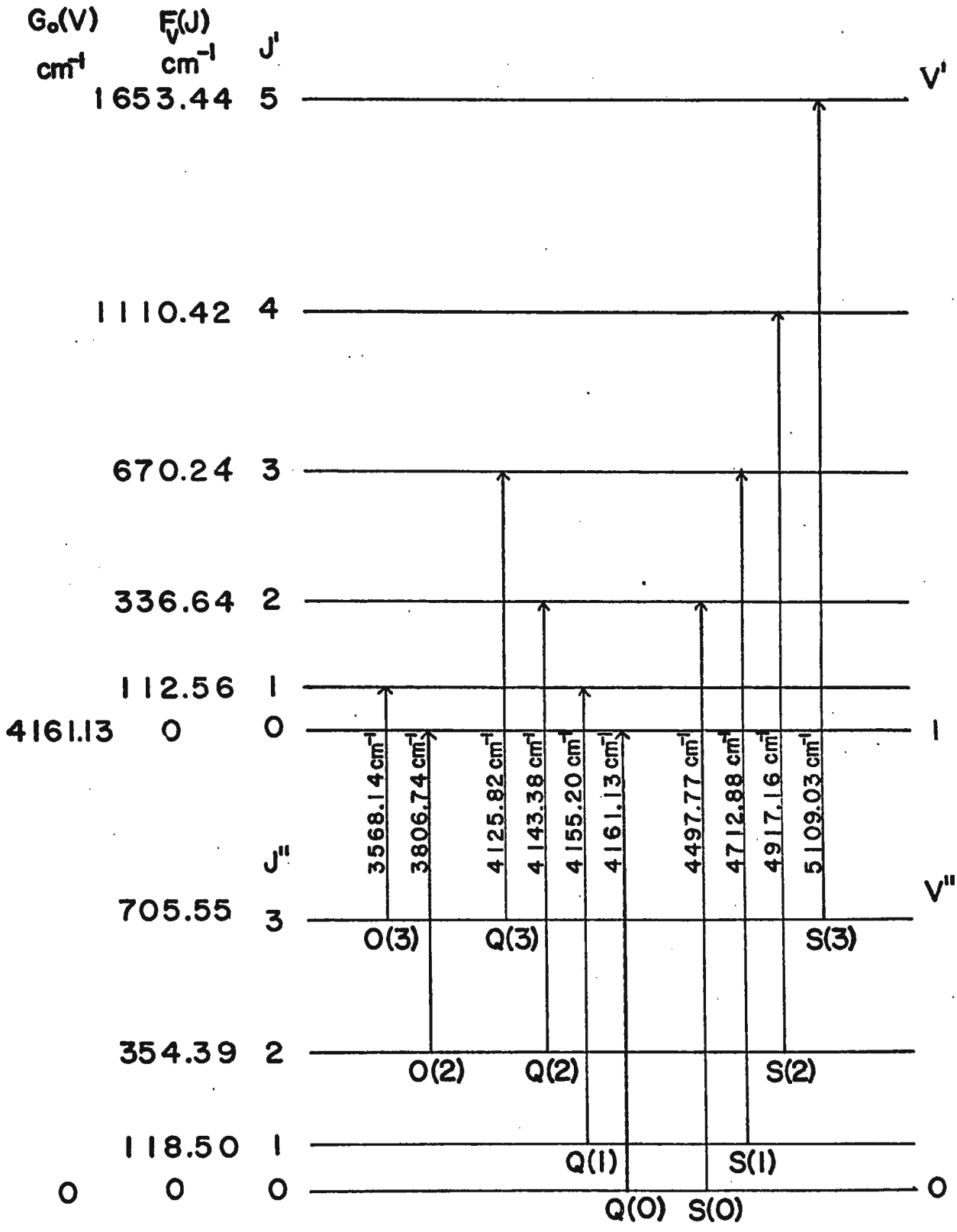

Fig.1. Single transitions in the induced fundamental band of hydrogen.

The theory of the collision-induced absorption of the fundamental bands of homonuclear diatomic gases was developed by Van Kranendonk and Bird (1951a, 1951b), Van Kranendonk (1957, 1958) and Britton and Crawford (1958). A detailed summary of the theory is presented in Appendix A. According to Van Kranendonk (1957, 1958) who used a simplified model for the dipole moment induced in a colliding pair of molecules by the intermolecular forces, the induced dipole moment consists of two components, the angle-independent short-range electron overlap dipole moment and the angle-dependent long-range quadrupole-induced dipole moment. The first component is dominant in very close collisions and it decreases exponentially with the intermolecular distance R. It contributes mainly to the intensity of the Q branch. The second component arises from the polarization of one molecule by the quadrupole field of the other and varies as R^{-4}. It contributes to the intensity of the O, Q and S branches. The quadrupolar contribution to the Q branch is referred to as the Q_Q component. The model for the induced dipole moment mentioned here is often referred to as the 'exp-4' model. When this 'exp-4' model and the Lennard-Jones intermolecular potential are used for the dipole moment and the intermolecular potential, respectively, of the colliding pairs of molecules, the binary absorption coefficient can be respresented as a summation of the overlap and quadrupolar terms. Theory shows that in the range of binary collisions, for the fundamental band, the long-range quadrupolar intensity depends on the quantity $(Q_1'\alpha_2)^2 + (\alpha_1'Q_2)^2$ and the short-range overlap intensity depends on the overlap parameters λ and ρ (for the definitions of these parameters, refer to Chapter 4).

The long-range quadrupolar part of the binary absorption coefficient can be calculated by using the known molecular parameters of the absorbing and colliding molecules. The parameters λ and ρ can be determined by fitting the theoretical binary absorption coefficient as a function of temperature to the experimental values of the binary absorption coefficient at several temperatures. For the pure hydrogen gas, this fit was performed by Hunt (1959) to the experimental values of the binary absorption coefficients at $195^{o}K$ and $300^{o}K$ and the values of λ and ρ were determined for the H_2-H_2 pairs. However, prior to the present work, this type of fit has not been done for the binary mixtures of H_2 with foreign gases because of the inadequacy of accurate values of the binary absorption coefficients over a wide temperature range.

The present investigation was designed to obtain reasonably accurate values of the binary absorption coefficients of the fundamental band of H_2 in H_2-He and H_2-Ne at four different temperatures in the range $77^{o}K$ - $298^{o}K$ and to estimate the overlap parameters λ and ρ of these two mixtures. The present work on H_2-He at $195^{o}K$ and $298^{o}K$ and on H_2-Ne at $298^{o}K$ is complementary to the work of the previous investigators at McLennan Laboratory, University of Toronto (Chisholm and Welsh 1954, Hare and Welsh 1958, Hunt 1959), and to that of Reddy and Lee (1968) in our laboratory, respectively. Since the polarizabilities of helium and neon are small and their quadrupole moments are zero, the main contribution to the absorption coefficient comes from the overlap parts (the reader will find in Chapter 3 of this thesis that the overlap part in these two mixtures contributes 84% to 97% of the total value of the

binary absorption coefficient in the temperature range $77^{o}K$ - $298^{o}K$). Moreover, since hydrogen, helium and neon remain gaseous down to very low temperatures, the two binary mixtures under consideration provide a unique opportunity to study the behaviour of the distortions of their electron clouds over a wide temperature range. Actually, the band was studied in the two mixtures for gas pressures up to 200 atm at $77^{o}K$, $195^{o}K$, $273^{o}K$ and $298^{o}K$. Integrated absorption coefficients were measured and the binary and ternary absorption coefficients were derived for the fundamental band of H_2 in each of the mixtures. The quadrupolar parts of the binary absorption coefficients were calculated using the molecular parameters of the gases. The overlap parts were obtained by subtracting these from the experimental values. The parameters λ and ρ were determined for each of the mixtures by obtaining the best fit of the theoretical overlap parts of the binary absorption coefficients as a function of temperature to the experimental values of the overlap parts.

CHAPTER 2

EXPERIMENTAL METHOD

The object of the present investigation was to obtain reasonably accurate binary absorption coefficients of the collision-induced fundamental band of hydrogen in H_2-He and H_2-Ne mixtures at different temperatures in the range 77^oK - 298^oK. A detailed description of the absorption cells, the optical arrangement, the high pressure gas handling system, etc., used in the present study is given in this chapter. Also included in this chapter is an account of the experimental procedure and of the isothermal data of experimental gases, and a note on the test for the linear response of the PbS detector used in the spectrometers.

2.1 High Pressure Gas Absorption Cells

(a) 1 m Absorption Cell: A transmission-type 1 m absorption cell was used to study the band at 298^oK, 273^oK and 195^oK in the binary mixtures of hydrogen with helium and neon at pressures up to 300 atm. The construction details of the absorption cell, the cooling jacket and the vacuum chamber attachments (Bishop 1966) are shown in Figs. 2 and 3. The cell A is a 303 stainless steel tube, 1 m long, 3/4 in. in inner diameter, with a wall thickness of 1/8 in. and with two flanges, F, hard-soldered at both ends. Each of the end pieces, B, also made of 303 stainless steel which is 3 in. in diameter and 5 in. long, was attached to the cell body by means of the steel closing nuts N_1. A stainless steel ring R_1 served to obtain a pressure-tight seal between the cell A

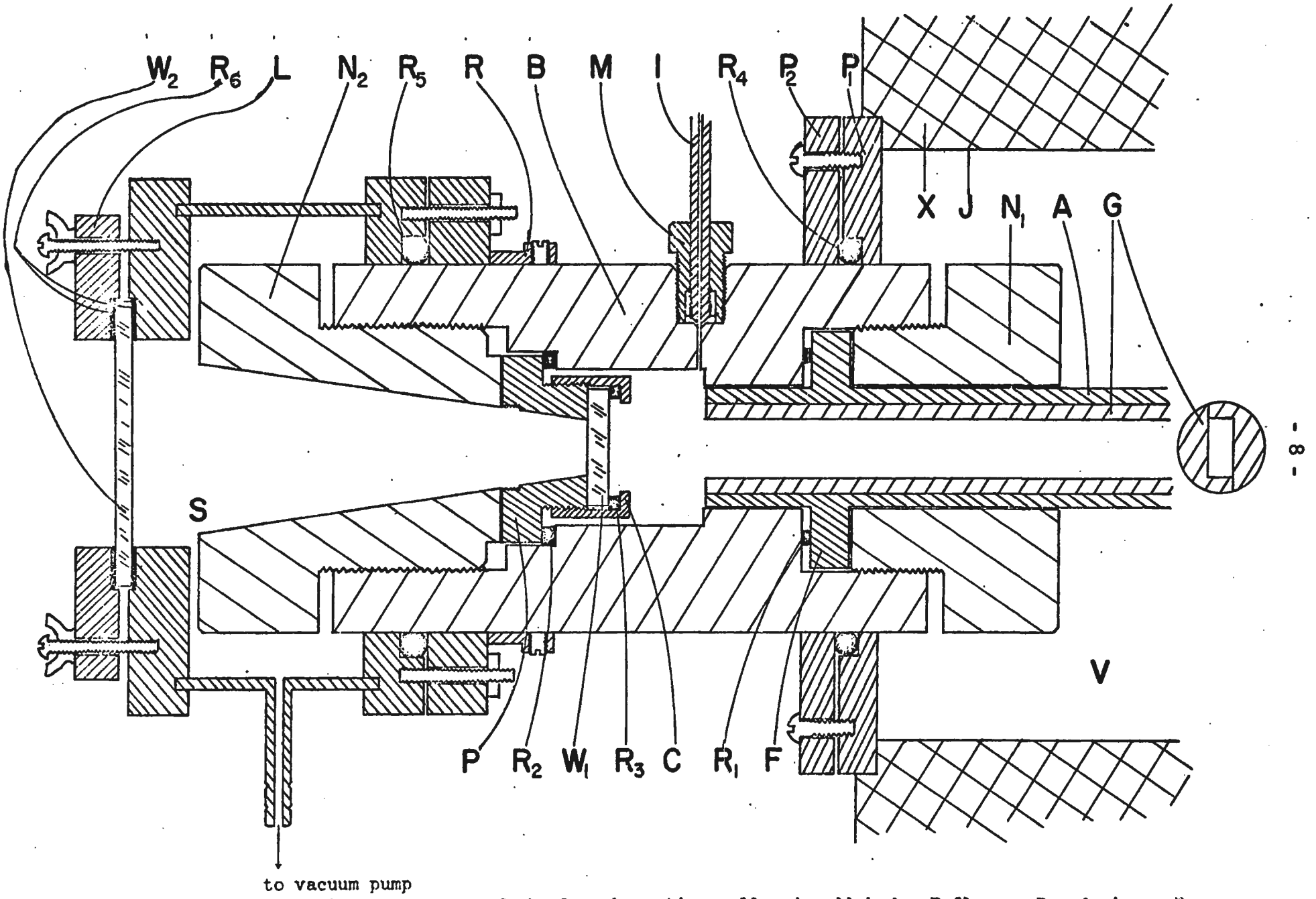

Fig. 2. A cross-section of one end of the 1 m absorption cell: A,cell body; F,flange; B,end piece; R_1, stainless steel ring; N_1,N_2,nuts; G,light guide; W_1,sapphire window; P,window plate; R_2,R_3,teflon rings; C,cap; I,capillary gas inlet; M,Aminco fitting; J,cooling jacket made of galvanized tin sheet;P_1,P_2, brass plates; R_4,R_5,neoprene "O" rings;R_6,rubber gaskets;W_2,quartz window; L, clamping arrangement; S,vacuum chamber; V, pumping space; X,styrofoam insulator; R,retaining ring.

and the end piece B. A stainless steel light guide G made in four sections (each section consisting of two parts) and having a central rectangular aperture 0.4 in. x 0.2 in. was inserted into the cell body. The inner surfaces of the light guide were polished to ensure high reflectivity of radiation. To obtain proper alignment between different sections of the light guide, a locking arrangement was provided for the adjacent sections. The entrance and exit windows W_1 were optically flat synthetic sapphire plates 1 in. in diameter and 5 mm thick. These were cemented to the optically flat window plates P by means of General Electric RTV-108 silicone rubber cement. The window plate holders have rectangular apertures 0.5 in. x 0.2 in. The windows were secured by steel caps C with teflon rings R_3 in order to prevent them from becoming loose during evacuation. A pressure-tight fit was obtained between the window plate P and the end piece B by using a teflon ring R_2 between them and by tightening the stainless steel nut N_2. To prevent misalignment of the window plate with the light guide while tightening the nut N_2, the end portion of the window plate was made into a square in shape to fit into a matched recess of the end piece B of the cell. A stainless steel capillary tube I, 1/4 in. in diameter, connected to the cell body by an Aminco fitting M, served as gas inlet.

For experiments at low temperatures the absorption cell was provided with a cylindrical jacket J, 3 3/8 in. in diameter, made of galvanized tin sheet (Fig. 3) to contain the coolants. Both ends of the jacket were soldered to circular brass plates P_1, having circular central holes that fitted the end pieces B (Fig. 2). The jacket was sealed around the end pieces of the cell by means of neoprene O-rings and by

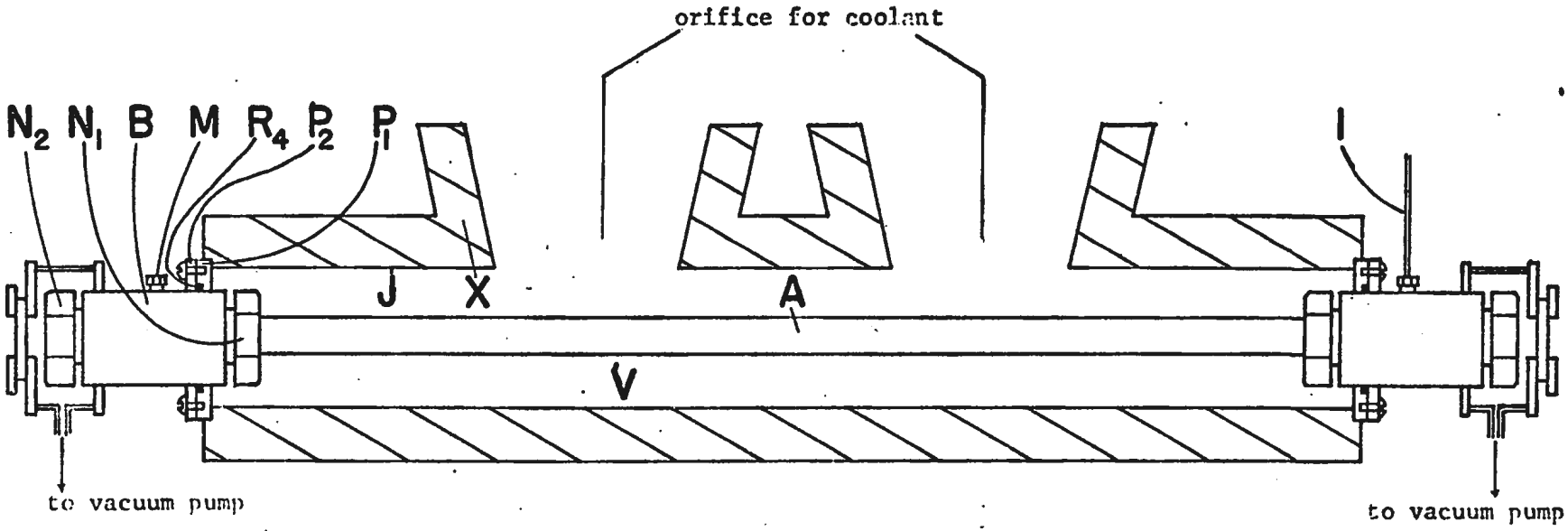

Fig. 3. 1 m absorption cell with its cooling jacket.
(See fig. 2. for the legend of the symbols.)

tightening the brass plates P_2 against P_1. The jacket was insulated by a 2 in. layer of styrofoam X.

To prevent frosting on the windows of the cell in the low temperature experiments, a vacuum chamber S, constructed of plexiglass (Fig. 2), was attached to each of the end pieces B of the cell. A square quartz window W_2, 2 in x 2 in. x 3 mm was sealed to the plexiglass by means of two rubber gaskets R_6 and by tightening eight screws into the clamping arrangement L. Retaining rings R were fastened by means of a set of screws to keep the vacuum chamber from slipping on over the end piece B of the cell when the chamber was evacuated. A neoprene O-ring R_5 was used to secure a vacuum seal down to 0.03 mm of Hg.

The coolants used with the 1 m absorption cell were crushed ice (273^oK) and dry ice-alcohol mixture (195^oK). The sample path lengths were 105.2 cm at 298^oK and 273^oK and 105.0 cm at 195^oK. The correction to the sample path length due to reflection in the light guide was estimated to be less than 2% and was not taken into account. The 1 m absorption cell could not be used for the work at liquid nitrogen temperature because of a serious distortion of the central tubing of the cell at this temperature. Initially, the cell was tested for pressures up to 400 atm at room temperature and up to 300 atm at 195^oK.

(b) 1/4 m Absorption Cell: The second absorption cell which was used for the work at liquid nitrogen temperature was also of the transmission type having a sample path length 26.7 cm at room temperature. The details of its construction (Sinha 1967) are shown in Fig. 4. The cell body A was constructed of a 303 stainless steel cylinder, 15.5 in. long, 3.2 in. in diameter, with a central bore of diameter 3/4 in. The

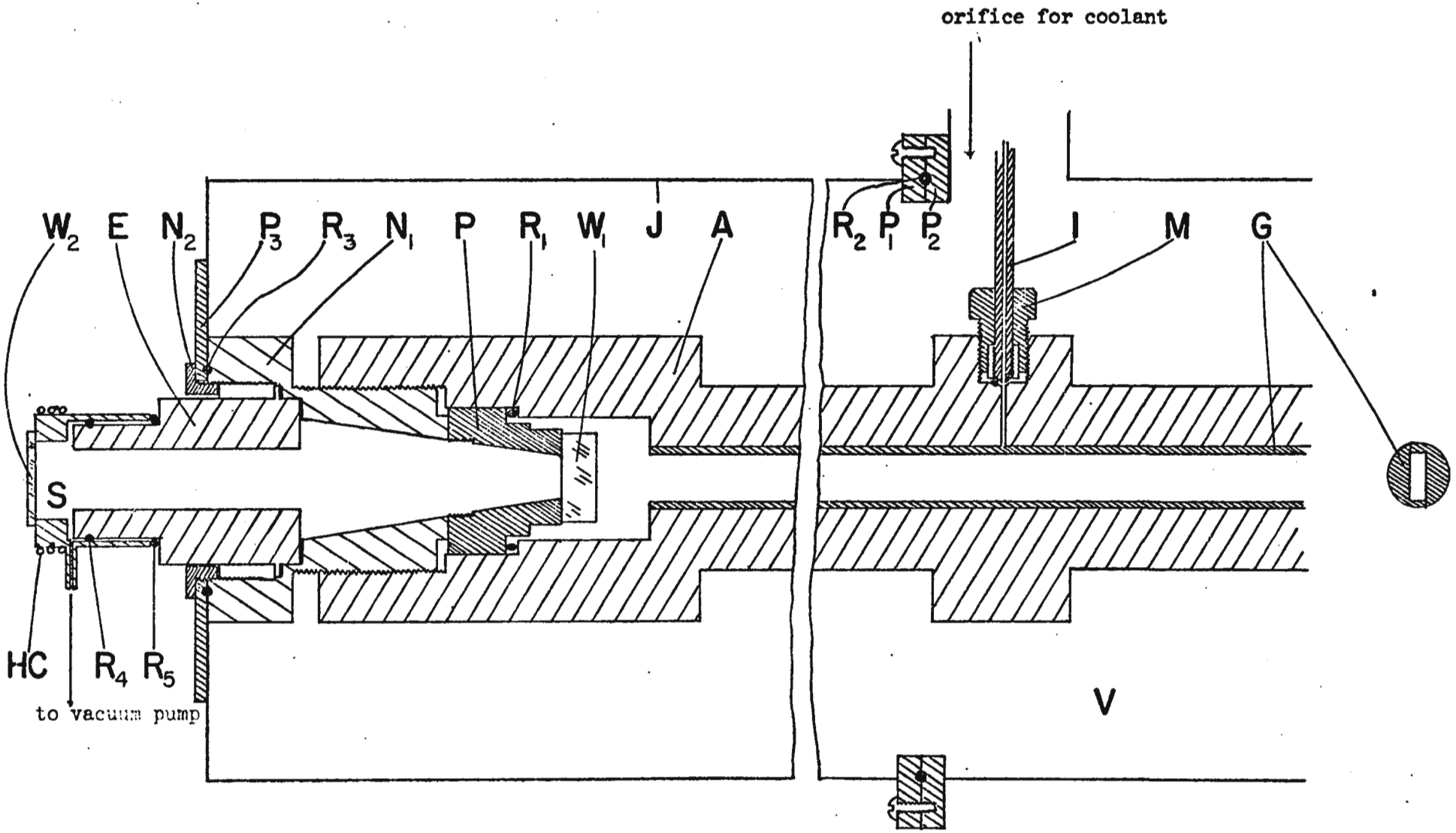

Fig. 4. The absorption cell used for work at liquid nitrogen temperature: A,cell body; G,light guide; W_1,W_2,sapphire windows; P,window plate; R_1,invar ring; N_1,N_2,nuts; I,capillary gas inlet;M, Aminco fitting; J,cooling jacket made of galvanized tin sheet; P_1,P_2,P_3,brass plates; R_2 to R_5, neoprene "O" rings;E,extension piece; S,vacuum chamber ; V, liquid nitrogen space; HC,heating coil.

stainless steel light guide G, made in two pieces, has a central rectangular aperture 3/8 in. x 3/16 in. and highly polished inner surfaces. The details of the window plate holders P, optical windows W_1, the cement used to attach W_1 to P, the capillary gas inlet I, etc., are similar to those described above for the 1 m absorption cell. In the present cell a high pressure seal between the cell body and the window plates was obtained by the use of invar rings R_1 in between them and by tightening the hexagonal nuts N_1. A cylindrical jacket J, made of tin sheet, was used to contain liquid nitrogen. A stainless steel extension E having a central bore of diameter 3/4 in. was provided to each of the nuts N_1 in the original design itself to fit a tubular plexiglass extension with a sapphire window W_2 in order to make a vacuum chamber S. The outer windows W_2 are optically flat synthetic sapphire plates 1 in. in diameter and 2 mm thick and were cemented on to the plexiglass extensions by General Electric glyptal cement.

The narrow bore of the extensions E unfortunately reduced the cones of the radiation entering and leaving the absorption cell to some extent. These extension pieces were cemented into the hexagonal nuts N_1. A leak proof seal between the brass plate P_3 of the jacket and the nut N_1 was obtained by means of the neoprene ring R_3 and by tightening the steel nut N_2. Vacuum-tight fitting between the plexiglass tube and the extension piece E was obtained by means of the rubber O-rings R_4 and R_5. Heating coils HC carrying a current of approximately 0.4 A prevented frosting on the outer windows. The cell was tested at pressures up to 400 atm at liquid nitrogen temperature. The sample path length of the cell was 26.6 cm at $77^{o}K$.

2.2 Optical Arrangement and Calibration of the Spectral Region

A schematic diagram of one of the optical arrangements used in the present investigation is shown in Fig. 5. A water-cooled tungsten filament lamp with a sapphire window, prepared in our laboratory (Kuo 1970) from a standard G.E. 750 watt projection bulb filament, served as a source of infrared radiation. The source was operated approximately at a power of 250 watts obtained from a stabilized a.c. power unit which was fed by a Sorenson ACR-2000 a.c. regulator. Radiation from the source S was focused on the entrance window of the cell H by a concave mirror M_1 and that from the exit window of the cell was focused by another concave mirror M_2 on the entrance slit of the spectrometer. Both M_1 and M_2 are aluminized spherical front surface mirrors having a radius of curvature of 60 cm each.

A Perkin-Elmer Model 112 single-beam double-pass spectrometer with a LiF prism was used to obtain the spectrum of the fundamental band of hydrogen at $195^{o}K$, $273^{o}K$ and $298^{o}K$ with the 1 m absorption cell. To obtain the spectrum at $77^{o}K$ with the 1/4 m absorption cell, a Perkin-Elmer Model 112 G single-beam double-pass spectrometer (Fig. 5) in the first order of a Bausch and Lomb grating with 300 lines/mm blazed at 3.0 μ was used. In both cases the detector was a PbS cell operated at room temperature.

The slits of the prism- and grating-spectrometers maintained respectively at 50 μ and 160 μ, gave spectral resolutions of ~ 4 cm^{-1} and 1.6 cm^{-1}, respectively, at 4161 cm^{-1}, the origin of the fundamental band of hydrogen. Light cones of f/4 were used throughout the optical

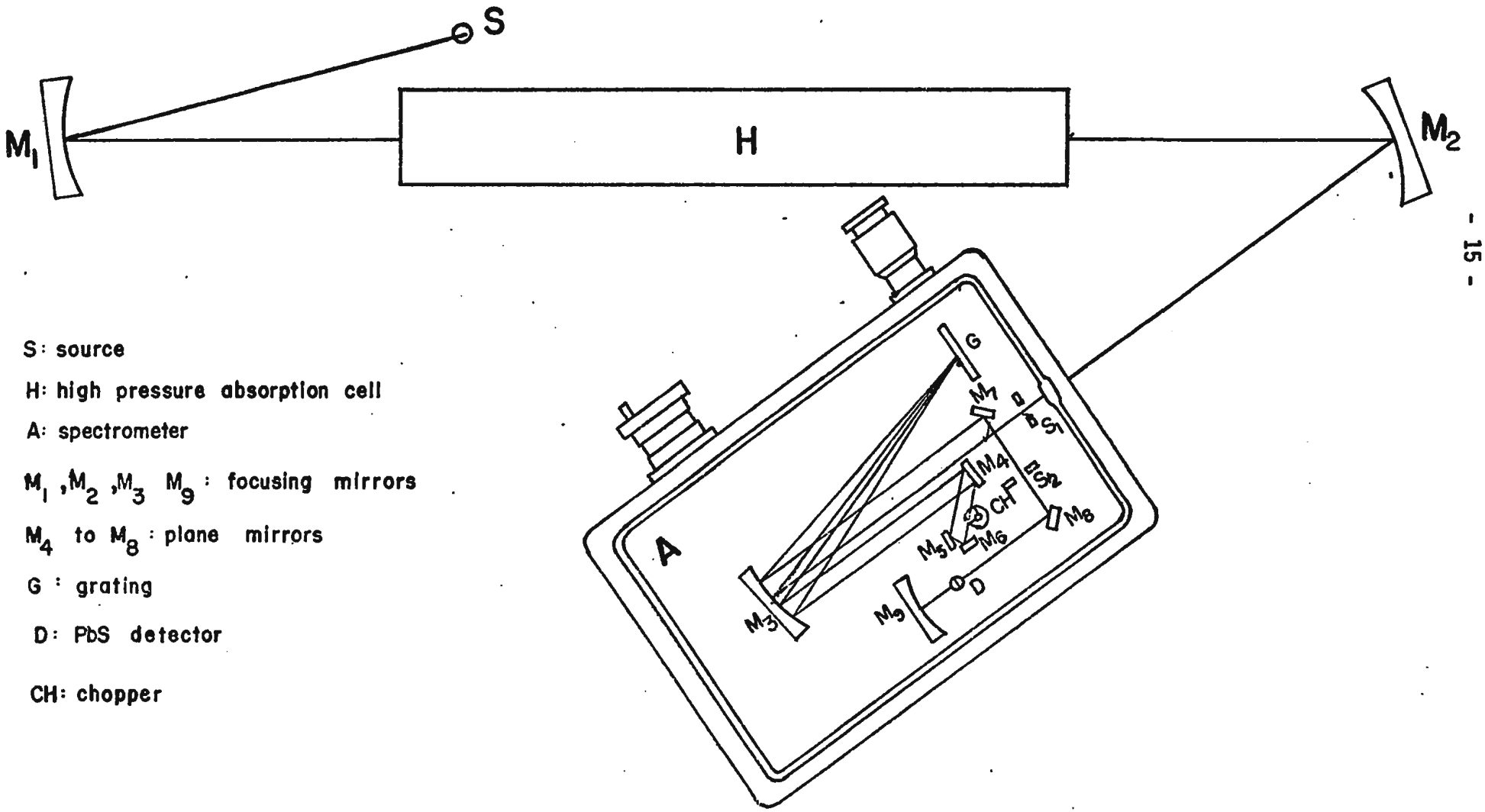

S: source

H: high pressure absorption cell

A: spectrometer

M_1, M_2, M_3 M_9 : focusing mirrors

M_4 to M_8 : plane mirrors

G : grating

D: PbS detector

CH: chopper

Fig.5. A schematic diagram of the optical arrangement

arrangements except in the case of the 1/4 m absorption cell. For the 1/4 m absorption cell the vacuum chambers at its ends were unfortunately narrow and hence only light cones of f/11 could reach the inner sapphire windows of the cell.

The spectral region of the fundamental band of hydrogen (3600 cm^{-1} - 6000 cm^{-1}) was calibrated using mercury emission lines (Humphreys 1953, I.U.P.A.C. Tables of Wave Numbers 1961), absorption peaks of atmospheric water vapor (Benedict and Plyler 1951, I.U.P.A.C. Tables 1961), 1, 2, 4-trichlorobenzene (Plyler, Blaine and Nowak 1957) and neon emission lines (Plyler, Blaine and Tidwell 1955).

Since the low- and high-frequency ends of the hydrogen fundamental band are overlapped by strong absorption of atmospheric water vapor present in the path of the optical beam, it was necessary to eliminate or reduce the water vapor in the optical path. In the present experiments this was done by enclosing the whole optical path, including the spectrometer, in a polyethylene enclosure and flushing continuously with carefully dried air.

2.3 Experimental Procedure

Figure 6 shows a schematic representation of the gas handling system used to introduce the gases into the absorption cell. In this figure, C is a mercury-column gas compressor which was used to compress the perturbing gas helium or neon to the required high pressures in the experiments at 77°K with the 1/4 m absorption cell. However, for the experiments at 298°K, 273°K and 195°K with the 1 m absorption cell, two thermal compressors C_1 and C_2 were used instead of the mercury-column

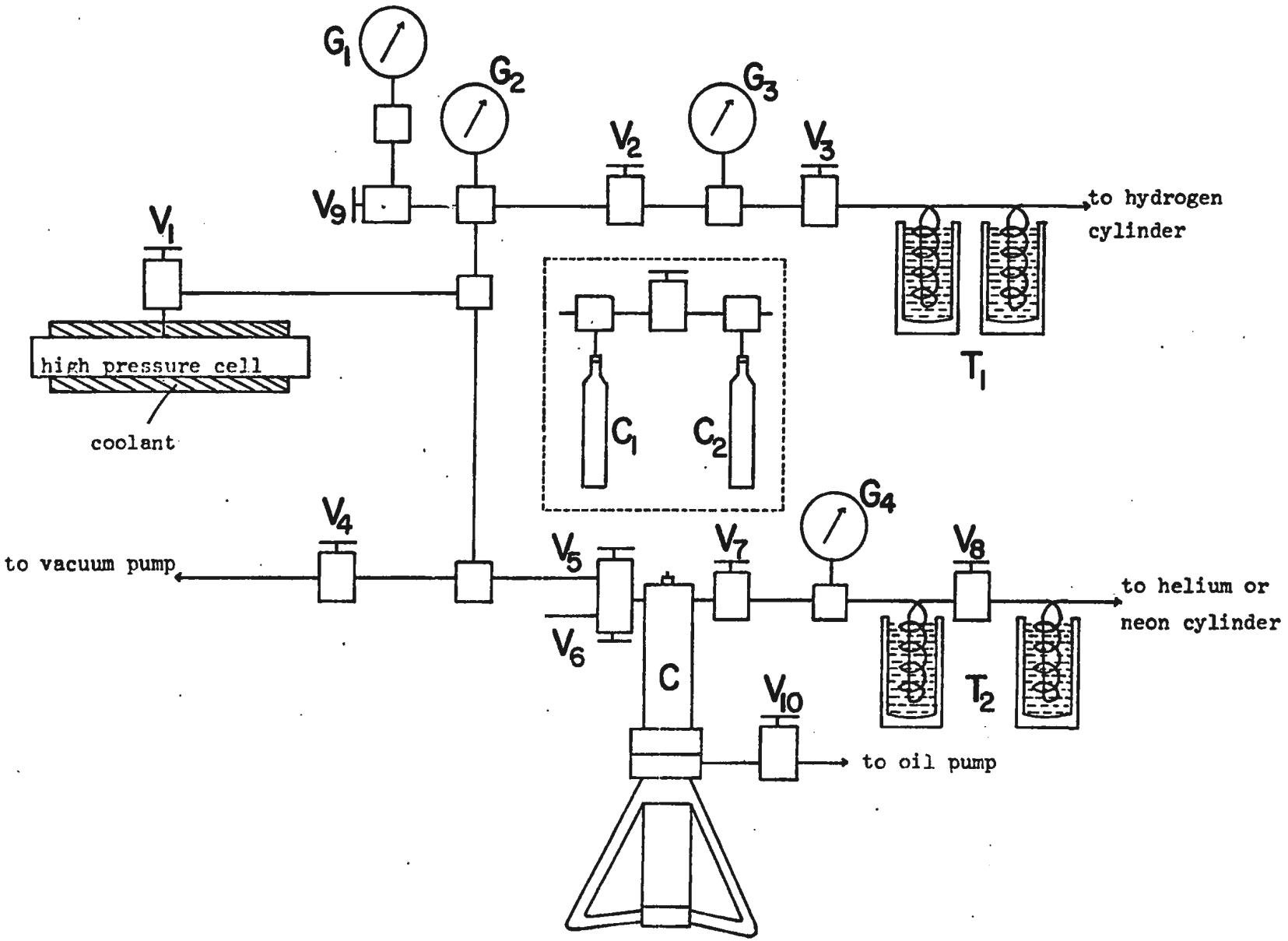

Fig.6. The gas handling system.

gas compressor. The coolant for the thermal compressors was liquid nitrogen.

In Fig. 6, V_1 to V_{10} are Aminco high pressure needle valves, T_1 and T_2 are liquid nitrogen traps made of copper tubing, 1/4 in. in outisde diameter, and G_1 to G_4 are Bourdon-type pressure gauges calibrated against an Ashcroft dead weight tester. Different components of the system were connected by stainless steel capillary tubing, 1/4 in. in outisde diameter. The length of the tubing between valve V_1 and the absorption cell was made as short as possible in order to reduce the error caused by hydrogen gas contained in that section. Prior to the actual experiments, the absorption cell and relevant parts of the gas handling system were tested for high pressures and for good vacuum for several days.

"Ultra-High Pure" hydrogen gas from a cylinder supplied by Matheson of Canada Limited was passed slowly through liquid nitrogen traps T_1 which served to eliminate impurities, if there were any, in the gas. For each mixture experiment the hydrogen gas was admitted into the evacuated absorption cell at a particular base pressure with valves V_4 and V_5 closed. The base pressure of hydrogen was read on gauge G_3 (which was one of 160-, 200-, 300-, 500-p.s.i. gauges). The valve V_1 was then closed and recorder traces of intensity I_1 for a given base pressure of hydrogen in the absorption cell were recorded until they were reproducible. For the mixture experiments at low temperatures it was found useful to admit a certain amount of hydrogen into the absorption cell before the cell was cooled. With valves V_1 and V_2 kept closed, the system was re-evacuated. The perturbing gas helium or neon (each of

which was 99.99% pure) from a cylinder supplied by Canadian Liquid Air was passed slowly through traps T_2 and required pressures of the gas were developed either in the mercury-column gas compressor driven by an Aminco hand-operated oil pump or in the thermal compressors. The perturbing gas was then admitted into the absorption cell to the required pressures in sharp pulses by opening valve V_1 momentarily three or four times at proper intervals. The pressure of the gas mixture in the cell was read on gauge G_1 (which is one of the 3000 p.s.i. and 5000 p.s.i. gauges) or G_2 (10,000 p.s.i. gauge) when the final momentary opening of V_1 showed no change in the pressure reading. When the pressure was higher than the range of G_1, valve V_9 was closed, and the reading was made on gauge G_2. Admission of a foreign gas in sharp pulses minimizes the back diffusion of hydrogen from the absorption cell. As observed by several earlier investigators (for example, Chisholm and Welsh 1954), the addition of a gas in sharp pulses caused a peculiar variation in the transmitted signal from the cell. The mixing of hydrogen with helium or neon was assumed to be complete when the deflection of the pen of the recorder regained its original level in a spectral region free from absorption, i.e., beyond the region of the fundamental band of hydrogen. The duration of mixing was found to be dependent upon the component gases of the mixture as well as upon the temperature of the cell. This duration was found to vary from 15 to 30 minutes for H_2-He and H_2-Ne binary mixtures. In general it was found to be longer at lower temperatures and for heavier perturbing gases. While admitting the compressed gas from the mercury-column gas compressor into the absorption cell, valve V_{10} was closed in order to prevent fluctuations of the mercury in the gas

compressor. In a given mixture experiment, the base pressure of hydrogen was kept constant in the absorption cell, and observations of absorption were taken for a series of pressures of the perturbing gas. For each pressure of the mixture, recorder traces of intensity I_2 were taken until a satisfactory reproduction was obtained. For experiments with helium or neon as a perturbing gas, several base densities of hydrogen, varying from 11 to 59 amagat, were used. During the experiments, the pen deflection for infinite absorption, i.e., for zero radiation entering the spectrometer, was checked several times.

In the experimental set up the spectrometer was not far from the low temperature jacket of the absorption cell. Since the PbS detector in the spectrometer was very sensitive to temperature it was found necessary, in the low temperature experiments, to allow sufficient time for the detector to attain a steady temperature before proceeding with the experiment.

2.4 Measurement of Enhancements of Absorption from the Experimental Traces

In the present investigation the enhancements in absorption of the fundamental band of hydrogen when the foreign gas helium or neon was admitted at a series of pressures into the absorption cell containing a fixed base pressure of hydrogen were of main interest. The enhancement in the absorption coefficient per unit path length $\alpha_{en}(\nu)$ at a given frequency $\nu(cm^{-1})$ due to the addition of a foreign gas at a density ρ_b into the absorption cell of length ℓ containing an absorbing gas at a fixed base density ρ_a is given by

$$I_2(\nu) = I_1(\nu) \exp[- \alpha_{en}(\nu)\ell] \tag{2-1}$$

where $I_1(\nu)$ is the intensity transmitted by the absorbing gas in the cell and $I_2(\nu)$ is the intensity transmitted by the binary gas mixture in the cell. From eq. (2-1), $\alpha_{en}(\nu)$ can be written as

$$\alpha_{en}(\nu) = \frac{2.303}{\ell} \log_{10}(I_1/I_2). \tag{2-2}$$

The recorder traces obtained in the experiment for several pressures of the mixture were plotted on the recorder trace obtained with the corresponding base pressure of hydrogen. Water absorption peaks at the low frequency end of the hydrogen fundamental band (around 3500 cm^{-1}) were used for frequency matching. A standard frequency chart showing the calibration peaks and a scale of wave numbers was prepared for the spectral region of the band. The traces were reduced with the help of a standard logarithmic scale by measuring $\log_{10}(I_1/I_2)$ at intervals of 5 cm^{-1} in the regions of the band origin and the S(1) line, and at intervals of 10 or 20 cm^{-1} in the rest of the spectral region of the band. The enhancement absorption profiles were obtained by plotting $\log_{10}(I_1/I_2)$ against ν. For some experiments, the values of I_1 and I_2 were read directly for each enhancement trace and the values of $\log_{10}(I_1/I_2)$ were derived later. The enhancements in the integrated absorption coefficient $\int\alpha_{en}(\nu)d\nu$ in cm^{-2} were derived from the areas under the enhancement absorption profiles.

2.5 Isothermal Data of Gases

The densities of gases used in the experiments were expressed in units of amagat which is the ratio of the density of a gas at a given temperature and pressure to its density at standard temperature and pressure (S.T.P.). The density of a gas expressed in amagat is directly related to the number density (i.e., the number of molecules per unit volume).

Hydrogen:

In the present experiments the densities of hydrogen at room temperature ($298^{o}K$) and ice temperature ($273^{o}K$) were obtained directly from its isothermal data given by Michels et al (1959). Its densities at dry ice-alcohol mixture temperature ($195^{o}K$) were calculated by the method of linear interpolation from the data at $173^{o}K$ and $198^{o}K$ also given by Michels et al (1959). Its densities at liquid nitrogen temperature ($77^{o}K$) for pressures up to 100 atm were obtained directly from the data given by Dean (1961). To calculate densities for pressures above 100 atm the following procedure was adopted. Michels et al represented P, V and ρ of hydrogen gas at any given temperature by the relation

$$PV = A + B\rho + C\rho^2 + D\rho^3 + E\rho^4 + F\rho^5 \qquad (2\text{-}3)$$

and gave the values of the coefficients A to F at different temperatures. The values of these coefficients at $77^{o}K$ were calculated by a least square polynomial fit of each of the coefficients as a function of temperature. Using the values of these coefficients thus obtained, P-ρ

data of hydrogen at 77°K for pressures above 100 atm were calculated. These data are summarized in Table I.

Helium:

The densities of helium at 298°K and 273°K were obtained directly from the isothermal data given by Michels and Wouters (1941). The densities of helium at 195°K and 77°K for pressures up to 100 atm were obtained directly from the data given by Mann (1962). The densities at these two temperatures for pressures above 100 atm were extrapolated using the equation (see American Institute of Physics Handbook, 1963, page 4-158)

$$PV = A_1 + B_1\rho + C_1\rho^2 \qquad (2\text{-}4)$$

in which the coefficients A_1, B_1 and C_1 were determined from the available P-ρ data up to 100 atm. The extrapolated P-ρ data for helium are also listed in Table I.

Neon:

The isothermal data of neon at 298°K and 273°K were obtained directly from Michels et al (1960). The data at 195°K and 77°K were determined from those at 190°K and 200°K, and 75°K and 80°K, respectively, given by Timmerhaus (1963).

2.6 The Partial Density of a Foreign Gas in a Binary Mixture

The partial density, ρ_b, of the foreign gas in a binary gas mixture was determined using the interpolation formula (see for example Reddy and Cho (1965)),

TABLE I

CALCULATED ISOTHERMAL DATA

HYDROGEN		HELIUM			
77°K		195°K		77°K	
P ATM	ρ AMAGAT	P ATM	ρ AMAGAT	P ATM	ρ AMAGAT
117	340	109	140	117	340
125	360	117	150	134	380
134	380	126	160	152	420
143	400	134	170	171	460
152	420	143	180	192	500
162	440	152	190	213	540
171	460	161	200		
181	480	170	210		
192	500	179	220		
202	520	188	230		
213	540	197	240		
224	560	206	250		

$$(2\text{-}5) \qquad \rho_b = \frac{1}{1+\beta'}\left[(\rho_a)_P + \beta'(\rho_b)_P\right] - \rho_a$$

where $(\rho_a)_P$ and $(\rho_b)_P$ are the densities of the absorbing gas (hydrogen) and the perturbing gas (helium or neon), respectively, at the total pressure P of the mixture, ρ_a is the density of hydrogen at the base pressure, and $\beta' = \rho_b'/\rho_a$ where ρ_b' is the approximate partial density of the perturbing gas corresponding to the partial pressure, $P_b = P - P_a$, P_a being the base pressure of hydrogen. The final value of ρ_b was obtained by the method of iteration.

2.7 Test for the Linear Response of the PbS Detector

In any spectrometer it is essential that the deflection recorded on the recorder traces be related linearly to the intensity of radiation falling on the detector. The linear response of the PbS detector used in the present study is verified in the following way. The spectrometer was set to a spectral frequency around 4700 cm^{-1}. A ground glass screen was placed in front of the entrance slit of the spectrometer and the screen was illuminated by a water-cooled tungsten filament lamp (described earlier), placed at about 30 cm away from the screen on the axis of the spectrometer. The voltage in the lamp was adjusted so that the radiant power finally falling on the detector did not exceed the limit specified on the recorder trace. The readings on the recorder trace were noted for several distances R between the lamp and the screen, as the lamp was moved farther away from the screen. These readings when plotted as a function of $1/R^2$ gave a reasonably good straight line which shows that the response of the PbS detector is linear within the accuracy of the measurements.

CHAPTER 3

EXPERIMENTAL RESULTS

The experimental apparatus described in the previous chapter was used to study the collision-induced fundamental band of hydrogen in binary mixtures of hydrogen with helium and neon at four different temperatures in the range 77°K to 298°K with absorption cells of sample path lengths 1/4 m and 1 m. The experiments were conducted for several base densities of gaseous hydrogen using perturbing gas densities up to 240 amagat in the 1 m cell and up to 510 amagat in the 1/4 m cell. Table II gives a summary of the experimental conditions for which the enhancement absorption profiles of the band were obtained.

TABLE II

SUMMARY OF EXPERIMENTS

Mixture	Temperature °K	Sample path length of the cell (cm)	Maximum density of the perturbing gas (amagat)	Number of mixture densities
H_2-He	298	105.2	160	24
"	273	105.2	240	39
"	195	105.0	210	16
"	77	26.6	450	14
H_2-Ne	298	105.2	90	17
"	273	105.2	100	15
"	195	105.0	180	16
"	77	26.6	510	20

In the following sections of the present chapter the enhancement absorption profiles of the H_2 fundamental band obtained in H_2-He and in H_2-Ne mixtures for different experimental conditions are presented, their features are discussed, and the binary and ternary absorption coefficients are derived.

3.1 Enhancement Absorption Profiles

(i) Profiles of H_2-He Mixtures:

Examples of typical sets of enhancement absorption profiles of the band obtained in H_2-He mixtures at 298°K, 273°K and 195°K with the 1 m cell and at 77°K with the 1/4 m cell are presented respectively in Figs. 7, 8, 9 and 10. In each of these figures the values of $\log_{10}(I_1/I_2)$ are plotted against frequency (cm^{-1}) for four representative total densities of the mixture with a fixed base density of hydrogen. The positions of the transitions O(2), Q(J) and S(J) with J = 0 to 3, calculated from the constants of molecular hydrogen obtained from the high resolution Raman data of the low pressure gas (Stoicheff 1957), are marked on the frequency axis.

In all these profiles the main dip of the Q-branch occurs at the position of the Q(1) Raman line (4155 cm^{-1}), as observed by the earlier investigators. The separation $\Delta\nu_{PR}^{max}$ between the peak positions of the main Q_P and Q_R components increases with the increasing density of the mixtures. It varies from 40 cm^{-1} to 90 cm^{-1}, 45 cm^{-1} to 120 cm^{-1}, 50 cm^{-1} to 90 cm^{-1} and 55 cm^{-1} to 105 cm^{-1} for the experimental contours presented in Figs. 7, 8, 9 and 10, respectively. It is seen that, as the temperature of the mixture is lowered, the intensity of the lower frequency component Q_P

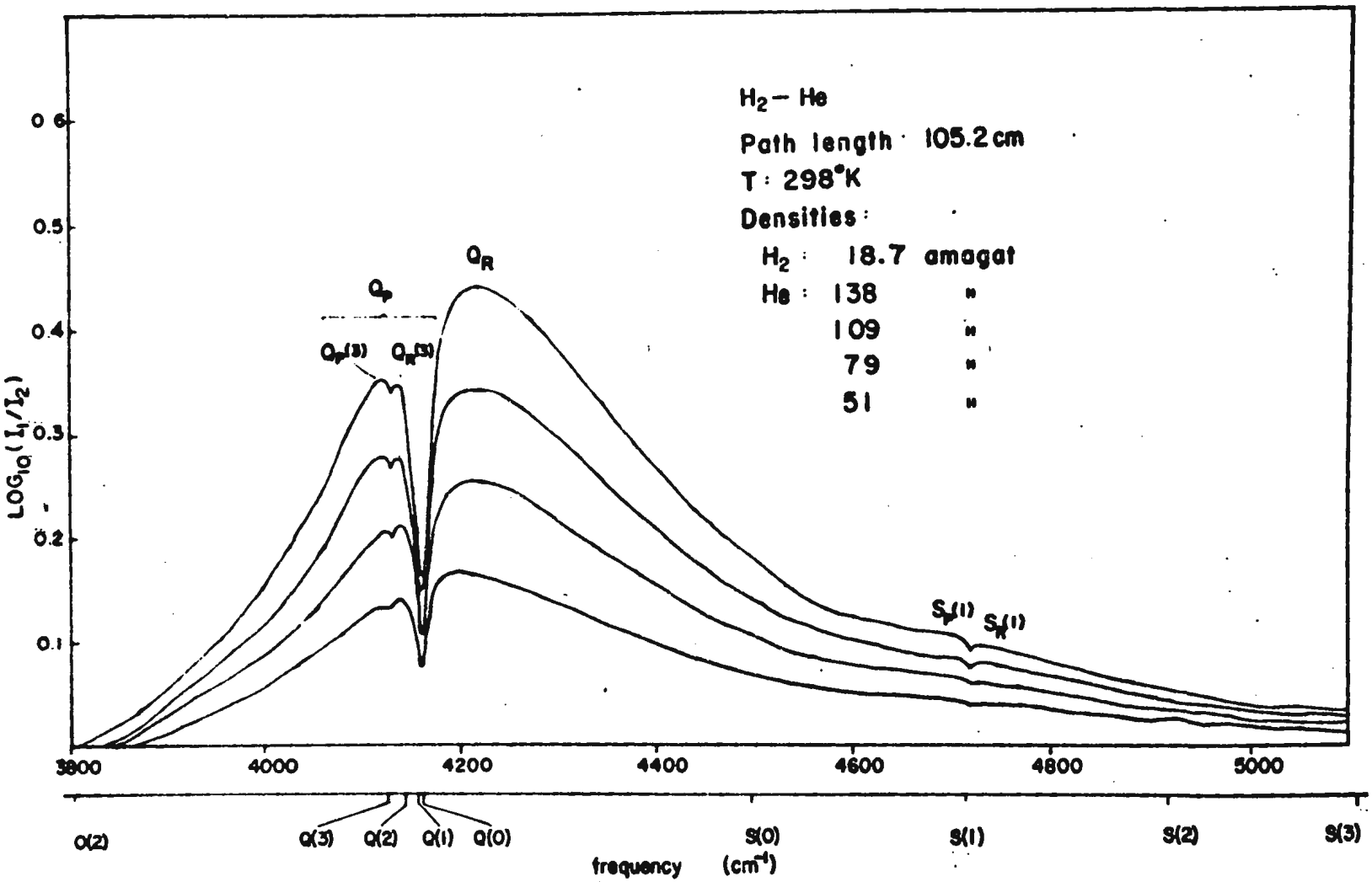

Fig. 7. Profiles of the enhancement of absorption of the fundamental band of H_2 in H_2 – He mixtures at 298°K.

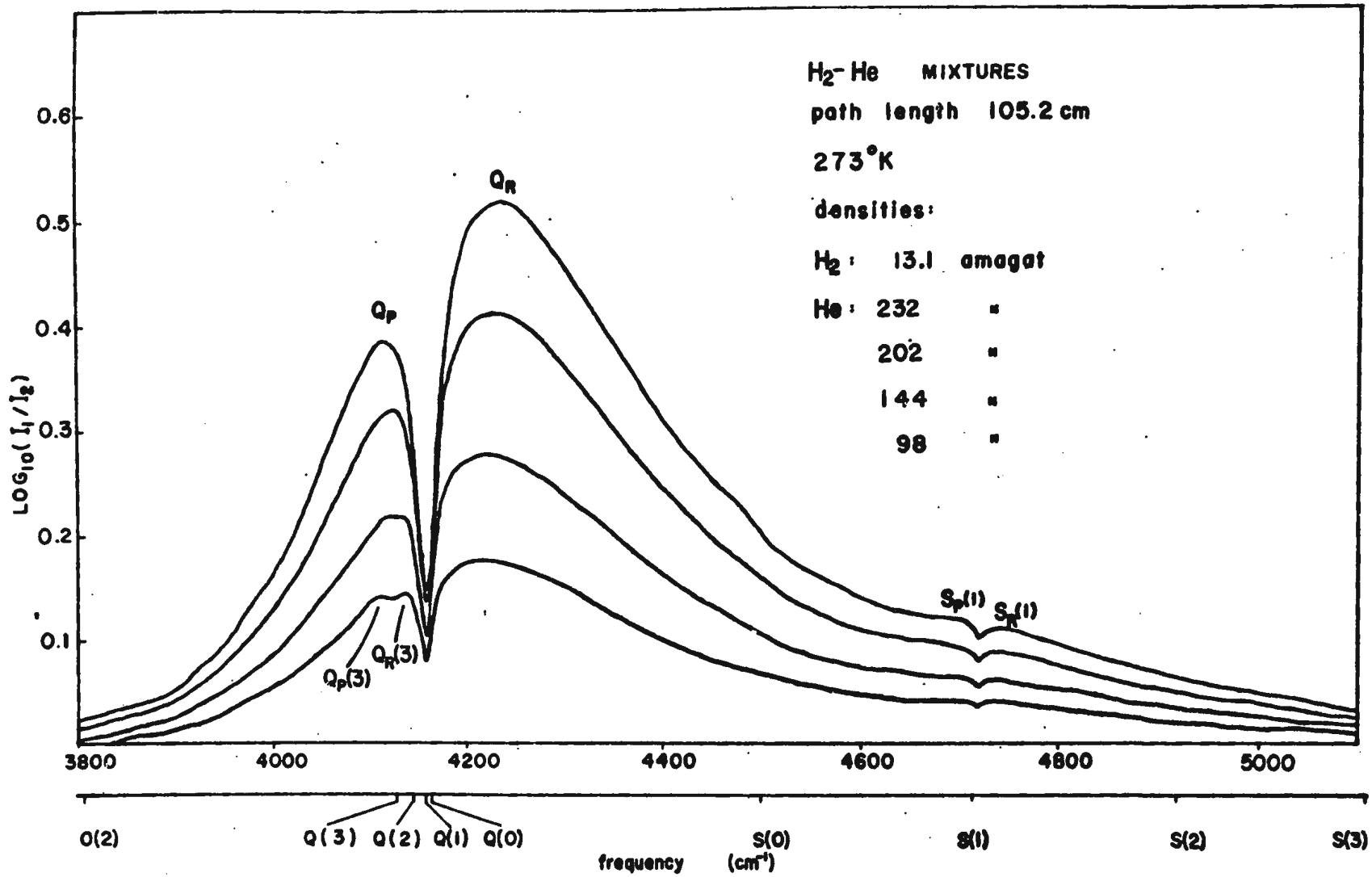

Fig. 8. Profiles of the enhancement of absorption of the fundamental band of H_2 in H_2 – He mixtures at 273 °K.

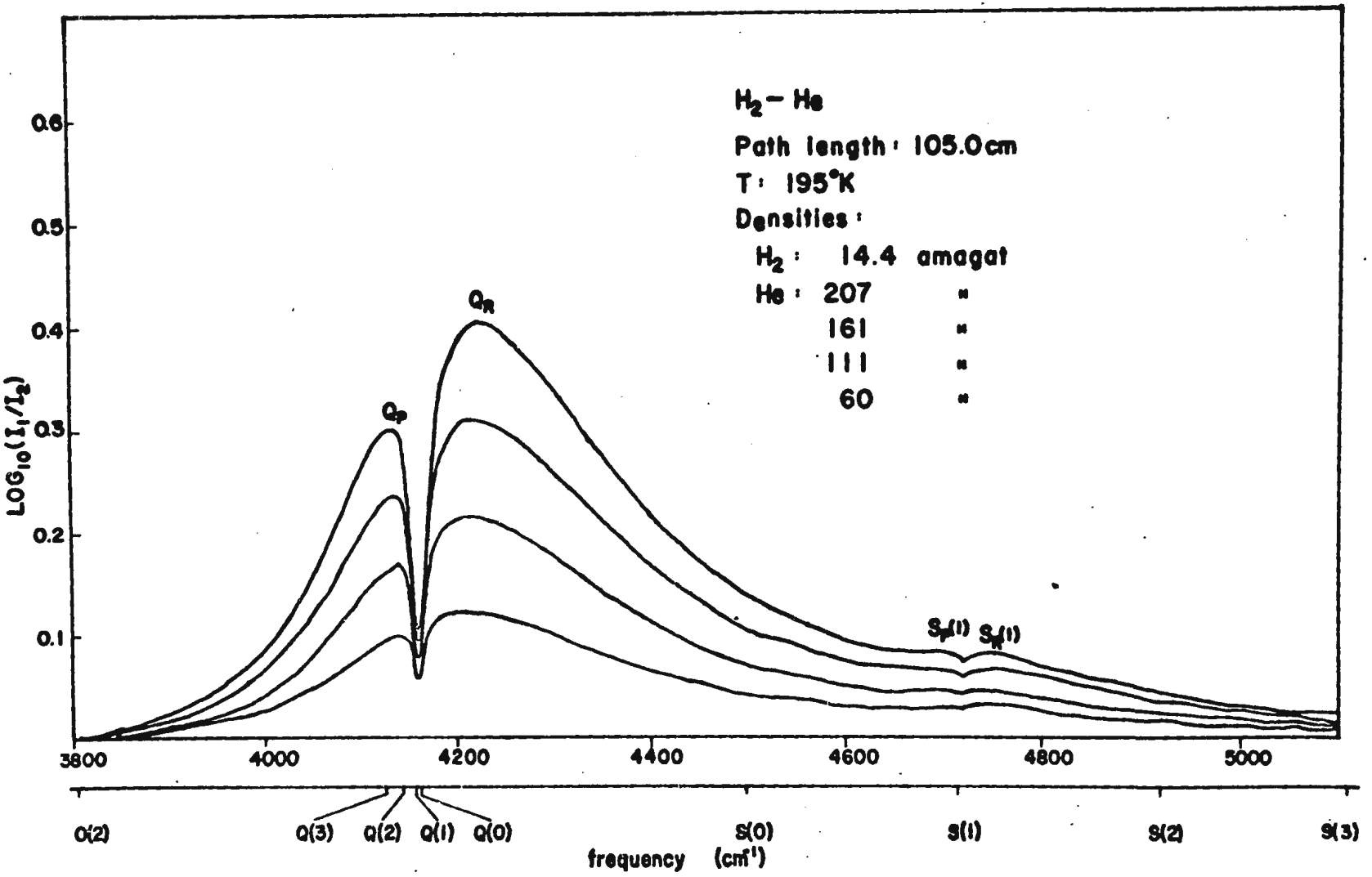

Fig. 9. Profiles of the enhancement of absorption of the fundamental band of H_2 in H_2 – He mixtures at 195°K.

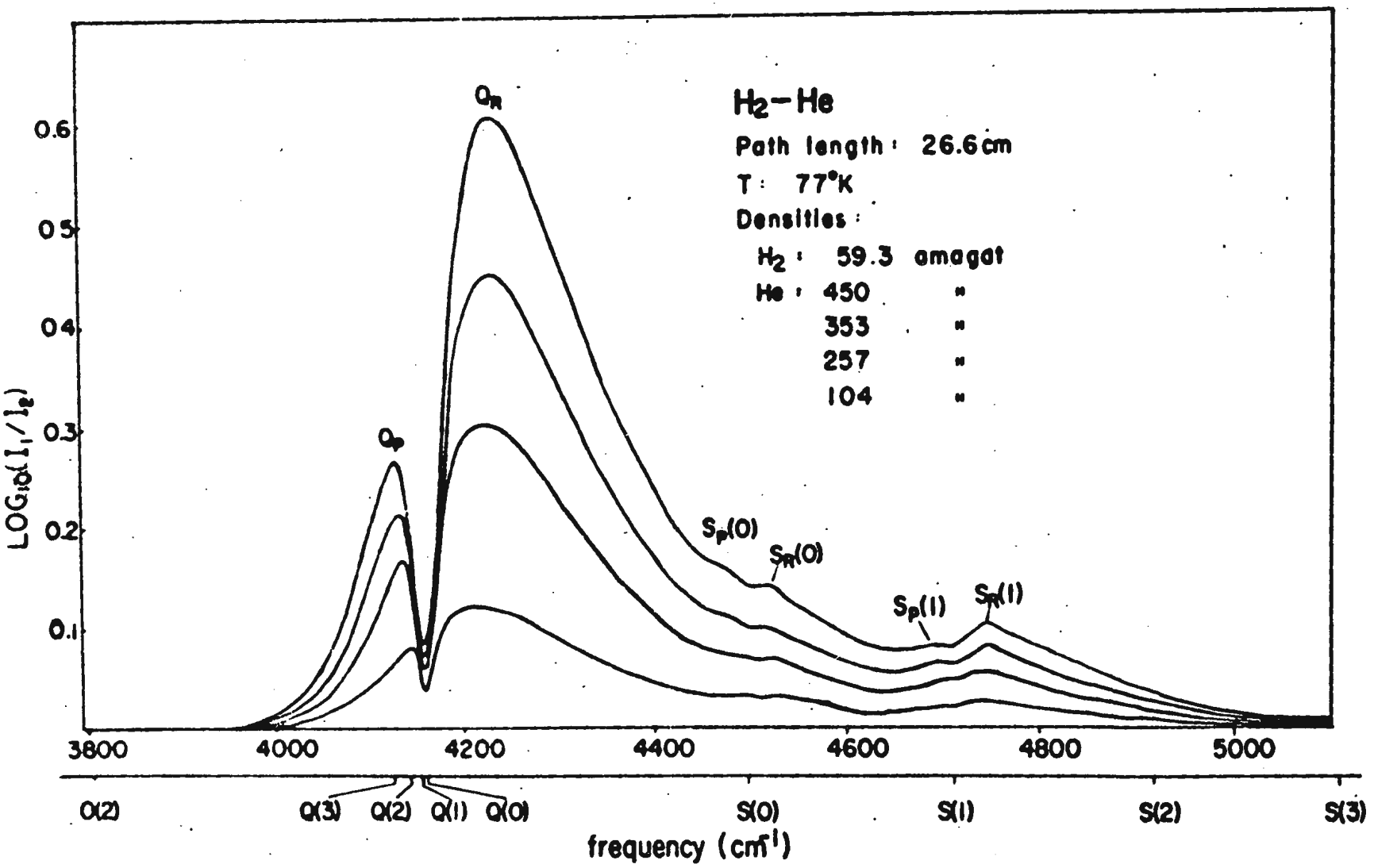

Fig. 10. Profiles of the enhancement of absorption of the fundamental band of H_2 in H_2 – He mixtures at 77 °K.

falls off more rapidly than that of the higher frequency component Q_R. This is because the lower frequency wing is modified by a Boltzmann factor (see Hunt and Welsh 1964; and Watanabe and Welsh 1967).

In addition to the usual main splitting of the Q branch into the Q_P and Q_R components at all experimental densities and temperatures in H_2-He, a secondary splitting of the main Q_P component occurs for all the contours at 298°K and for the contours at lower densities of the mixtures at 273°K. As the minimum of this splitting occurs at the position of the Q(3) Raman line (4126 cm^{-1}), its low- and high-frequency components are referred to as $Q_P(3)$ and $Q_R(3)$. The observation of the secondary dip at the position of the Q(3) line suggests that each one of the components of the $Q_{overlap}(J)$ (J = 0, 1, 2, 3, ...) of the Q branch has a profile similar to the Bjerrum double band with the dip occurring at the corresponding molecular frequency Q(J). The minima corresponding to Q(0) (4161 cm^{-1}) and Q(2) (4143 cm^{-1}) do not appear on the experimental traces because of their closeness to the more intense Q(1) line (4155 cm^{-1}) and of the broad nature of the overlap components (see Gush et al 1957; Reddy and Lee 1968). It is seen from Fig. 7 that the intensity of $Q_P(3)$ is less at lower densities and more at higher densities than the corresponding intensity of $Q_R(3)$. This can be explained on the basis of the increase in the peak separations of the individual $Q_P(J)$ and $Q_R(J)$ components (see below) with increasing density of the mixture. For the contours at 273°K the splitting of the $Q_{overlap}(3)$ component into $Q_P(3)$ and $Q_R(3)$ disappears as the density of the mixture is increased.

The striking feature of the S(1) line at all the four experimental temperatures (Figs. 7 to 10) is its splitting into the low- and high-frequency

components $S_P(1)$ and $S_R(1)$ with the minimum occurring at the position of the calculated S(1) Raman line (4713 cm^{-1}). This splitting of the profiles at lower densities at 77°K (Fig. 10) is not well pronounced; at lower densities the $S_R(1)$ peak occurs at positions about 35 to 40 cm^{-1} higher than that of the S(1) Raman line with no indication of the $S_P(1)$ peak (also refer to page 41).

For the profiles of H_2-He at higher densities in the experiments at 77°K (Fig. 10), there is a clear indication of the splitting of the S(0) line into $S_P(0)$ and $S_R(0)$ components with the minimum between them occurring at the position of the calculated S(0) Raman line (4498 cm^{-1}). It is the first time that such a dip has been observed for the S(0) line of the collision-induced fundamental band of H_2.

It will be seen in the next section of this chapter that the ternary absorption coefficients for the experimental binary mixtures are very small compared to the binary coefficients. Therefore, most of the intensity of the induced absorption at moderate densities of the mixture can be considered as a contribution by the binary collisions. In order to compare the overall absorption arising from the binary collisions between H_2 and He molecules at different temperatures, a comparison of the enhancement absorption profiles of H_2-He mixtures at 298°K, 273°K, 195°K and 77°K is made in Fig. 11. The profiles in this figure were chosen such that the products $\ell\rho_a\rho_b$ are approximately the same. Here ℓ is the sample path length of the cell, ρ_a is the density of the hydrogen gas and ρ_b is the density of helium (perturbing) gas. As the temperature of a mixture is lowered, the higher rotational states of the absorbing molecules would be depopulated and the translational energy of the

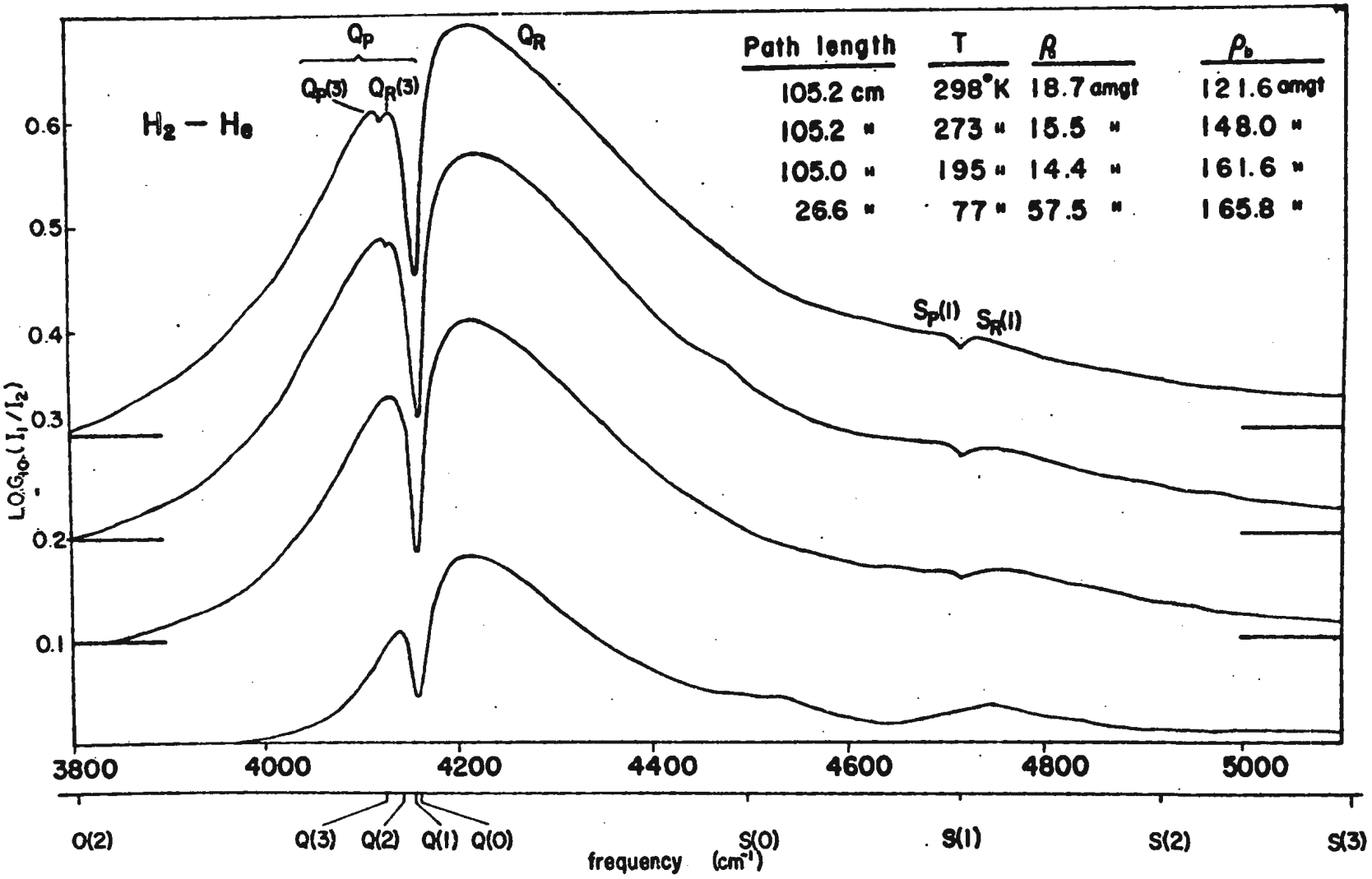

Fig. 11. Comparison of the enhancements of absorption of the fundamental band of H_2 in H_2 – He mixtures at different temperatures.

component gases would be decreased. The width of the absorbing lines depends on the duration of the collisions between molecules. At higher temperatures when the translational energy of the colliding pairs is large, the duration is small so that the lines are broad. Since the duration is greater at lower temperatures, the lines are, in general, sharper. This effect of low temperature on a mixture is clearly seen in the profile obtained at $77^{o}K$ (Fig. 11).

(ii) Profiles of H_2-Ne Mixtures:

Representative sets of enhancement absorption profiles of the H_2 fundamental band obtained in H_2-Ne mixtures at $298^{o}K$, $273^{o}K$ and $195^{o}K$ with the 1 m cell and at $77^{o}K$ with the 1/4 m cell are given in Figs. 12, 13, 14 and 15, respectively.

The behaviour of the main splitting of the Q branch into Q_P and Q_R in H_2-Ne mixtures at all the four experimental temperatures is similar to that discussed above for the H_2-He mixtures. For the experimental profiles presented in Figs. 12, 13, 14 and 15, the separation $\Delta\nu_{PR}^{max}$ increases from 35 to 85 cm^{-1}, 40 to 80 cm^{-1}, 40 to 85 cm^{-1} and 45 to 110 cm^{-1}, respectively, as the total densities of the mixtures are increased. One addiational feature of the Q branch in H_2-Ne mixtures at $77^{o}K$ is the appearance of the (quadrupolar) Q_Q component at high densities of the mixture (Fig. 15). At $77^{o}K$, only the two lowest rotational states J = 0 (para H_2) and J = 1 (ortho H_2) are populated. For the enhancement absorption profiles of the band in binary mixtures of hydrogen with monoatomic perturbing gases, only single transitions can occur for the Q_Q components as well as for the S lines. Since the quadrupolar single

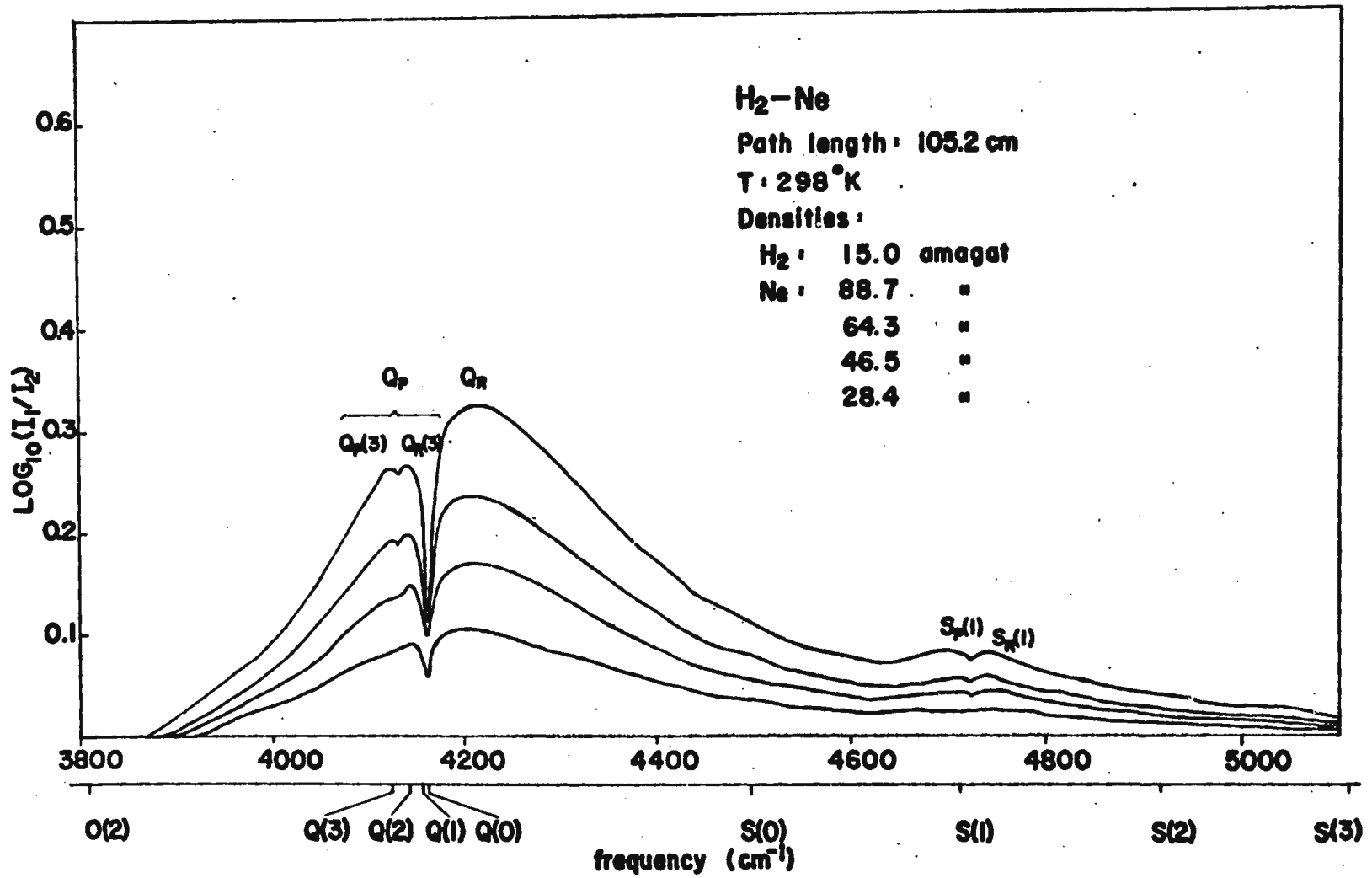

Fig. 12. Profiles of the enhancement of absorption of the fundamental band of H_2 in H_2 – Ne mixtures at 298 °K.

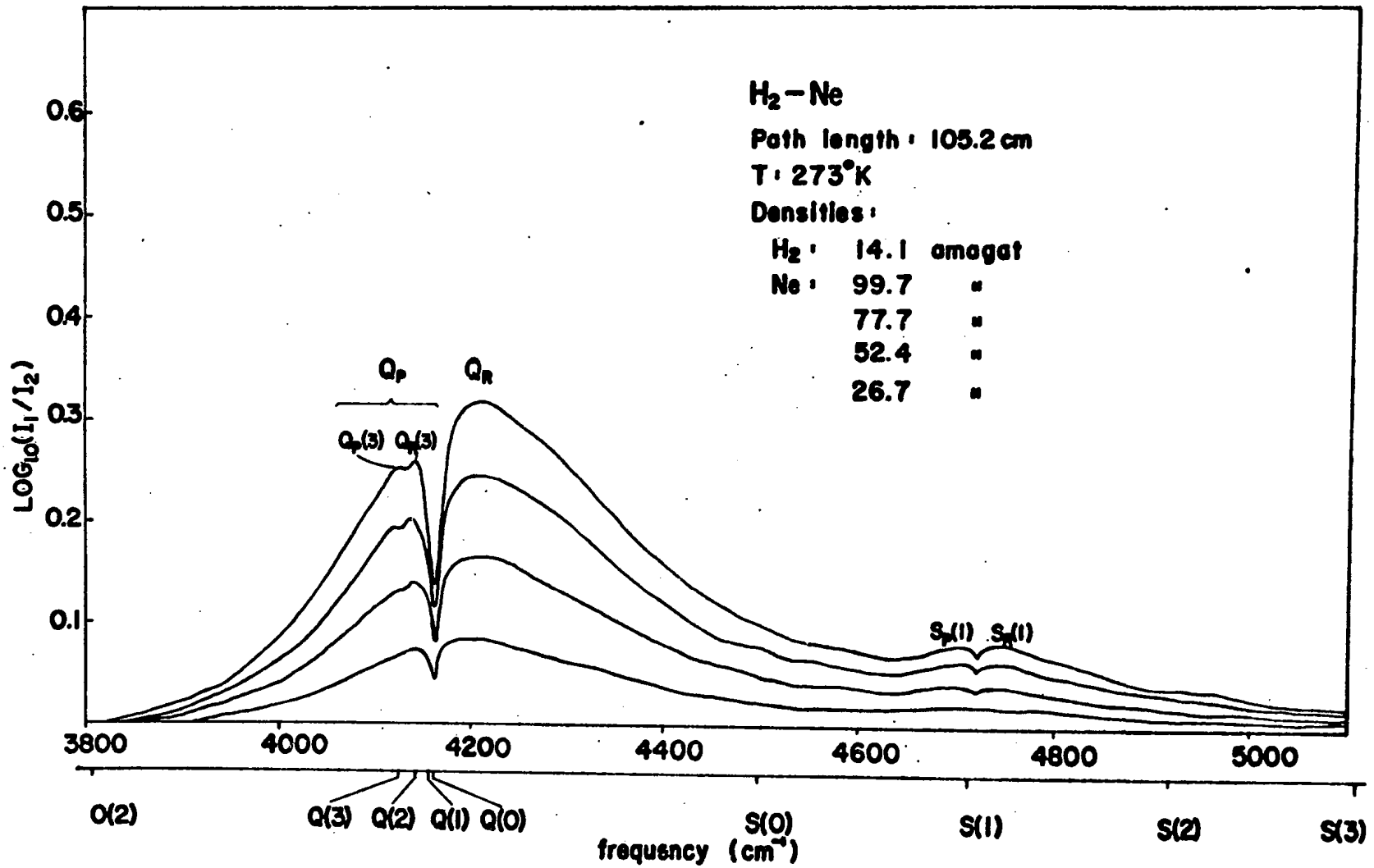

Fig. 13. Profiles of the enhancement of absorption of the fundamental band of H_2 in H_2 – Ne mixtures at 273°K.

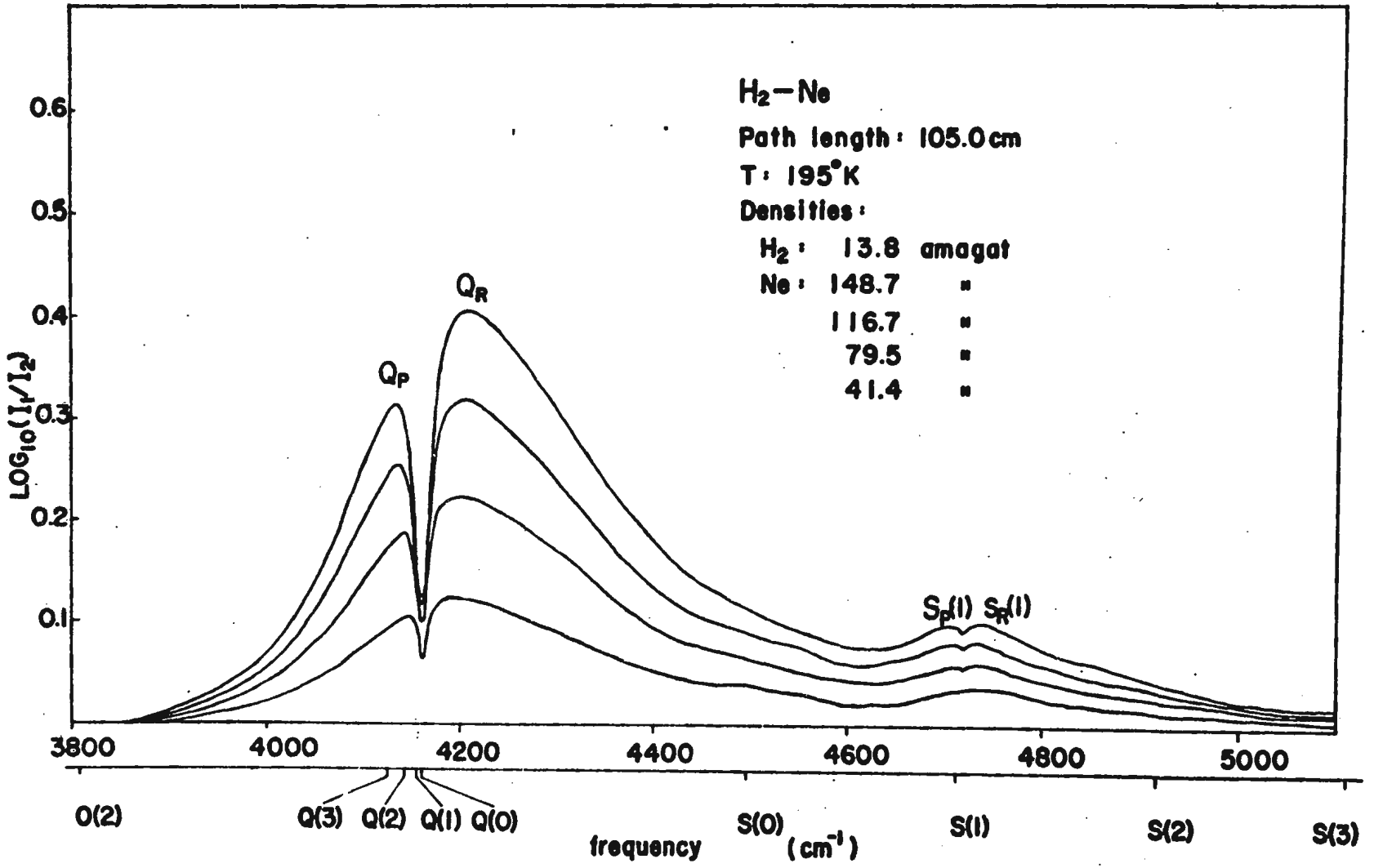

Fig. 14. Profiles of the enhancemt of absorption of the fundamental band of H_2 in H_2 – Ne mixtures at 195°K.

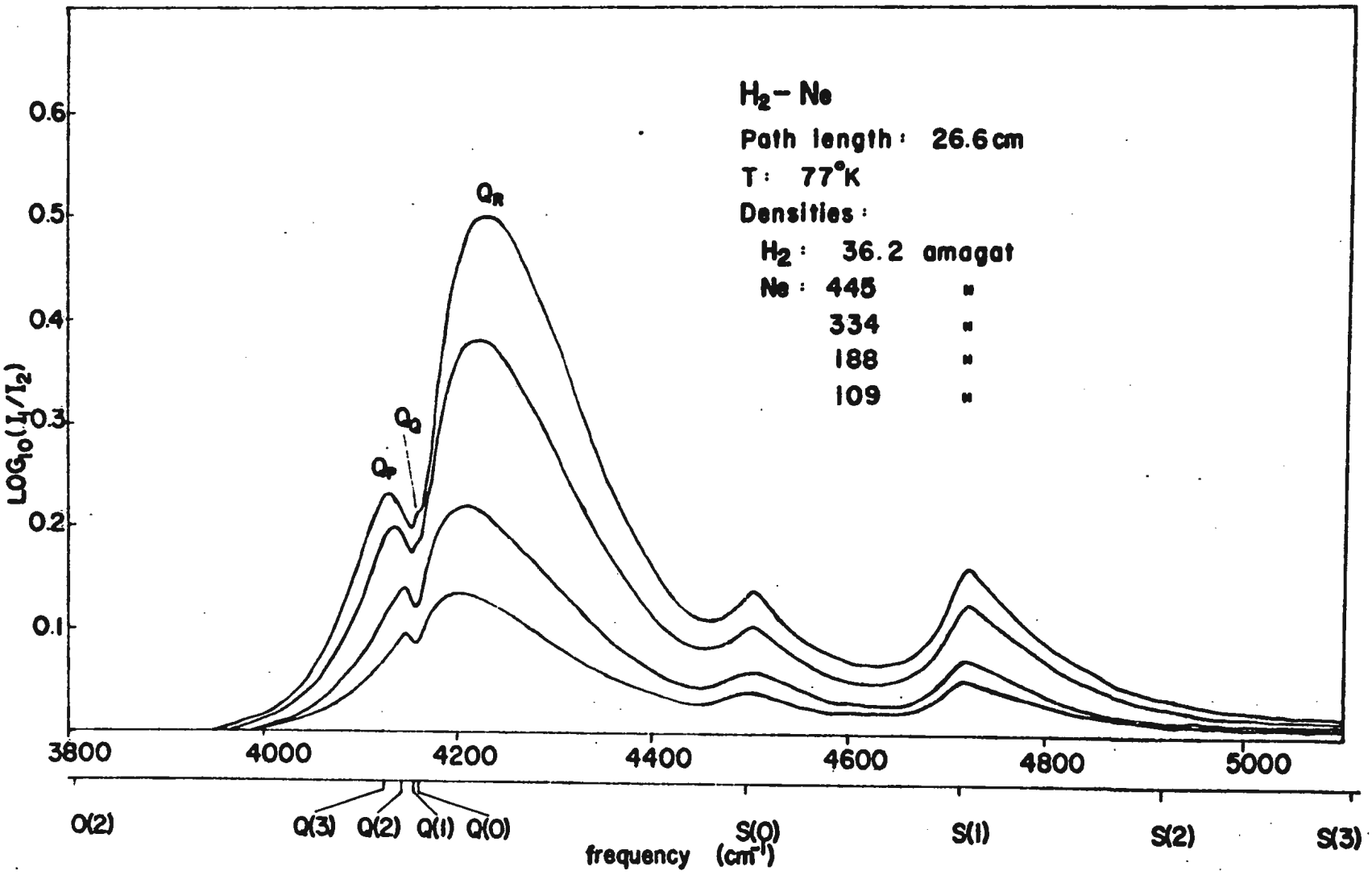

Fig. 15. Profiles of the enhancement of absorption of the fundamental band of H_2 in H_2 – Ne mixture at 77°K

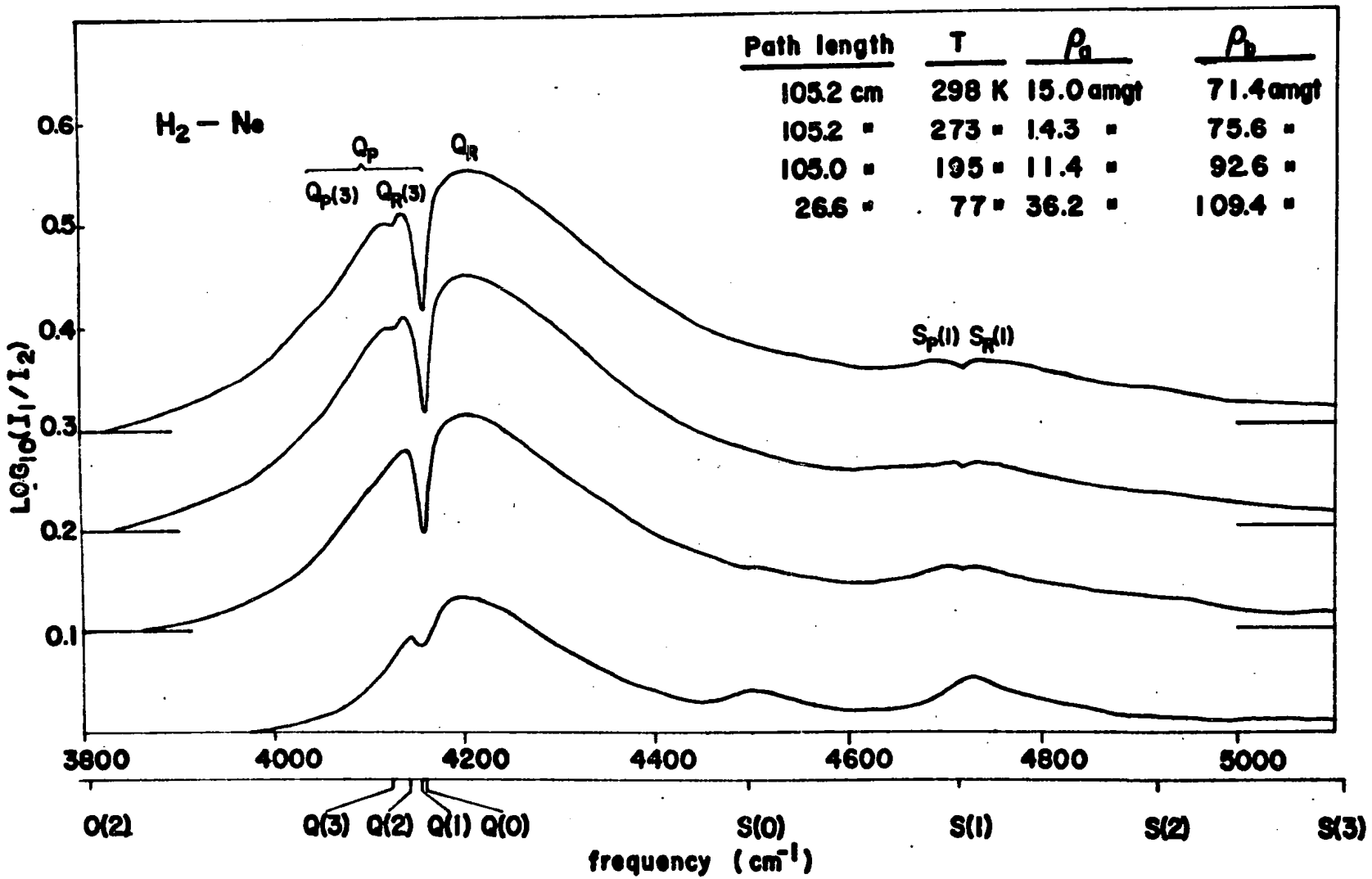

Fig. 16. Comparison of the enhancements of absorption of the fundamental band of H_2 in H_2 - Ne mixtures at different temperatures.

transition $J = 0 \rightarrow J' = 0$ is forbidden, the only quadrupolar component that occurs at 77°K is $Q_Q(1)$.

The splitting of the main Q_P component of the Q branch into $Q_P(3)$ and $Q_R(3)$ is also observed for the profiles of H_2-Ne at 298°K and 273°K for higher densities of the mixtures (Figs. 12 and 13). The splitting of the S(1) line into $S_P(1)$ and $S_R(1)$ is very marked at 298°K, 273°K and 195°K. The separation between these two peaks appears to increase with the increasing density of the mixture. It may be mentioned here that the components $Q_P(3)$, $Q_R(3)$, $S_P(1)$ and $S_R(1)$ for the H_2-Ne mixtures at room temperature were first observed by Reddy and Lee (1968). In the profiles at 77°K, the S(0) and S(1) lines are well pronounced and no splitting is observed for these. The peaks of the S(0) and S(1) lines occur respectively about 5 cm^{-1} and 10 cm^{-1} higher than the position of the S(0) and S(1) Raman lines. These peaks correspond to the high frequency components $S_R(0)$ and $S_R(1)$. The low frequency components $S_P(0)$ and $S_P(1)$ are too weak to be observed. This is because the intensity of a line falls off more rapidly on the low frequency side than on the high frequency side as the temperature of the mixture is lowered. A comparison of the enhancement absorption profiles of H_2-Ne at the four experimental temperatures is made in Fig. 11.

3.2 The Absorption Coefficients

The enhancements of the integrated absorption coefficients per unit path length $\int \alpha_{en}(\nu)d\nu$ (cm^{-2}) for H_2-He and H_2-Ne mixtures were obtained by numerical integration of the areas under the experimental profiles. The partial densities, ρ_a of hydrogen and ρ_b of helium or neon used in different experiments at each of the experimental temperatures and the corresponding values of $\int \alpha_{en}(\nu)d\nu$ and $(1/\rho_a\rho_b)\int \alpha_{en}(\nu)d\nu$ for H_2-He

and H_2-Ne mixtures are listed in Tables III and IV, respectively. The enhancements of the integrated absorption coefficients show a dependence on the partial densities ρ_a and ρ_b at all experimental temperatures for both H_2-He and H_2-Ne, which is given by the relation

$$\int \alpha_{en}(\nu)d\nu = \alpha_{1b}\rho_a\rho_b + \alpha_{2b}\rho_a\rho_b^2 + \cdots\cdots \quad , \tag{3-1}$$

where α_{1b} and α_{2b} are the binary and ternary absorption coefficients, respectively. The values of $(1/\rho_a\rho_b)\alpha_{en}(\nu)d\nu$ for H_2-He and H_2-Ne were plotted against ρ_b in Figs. 17 and 18, respectively. All the plots are straight lines, the intercepts giving the binary absorption coefficients and the slopes giving the ternary absorption coefficients. The values of these coefficients obtained by a least square fit of the experimental data are listed in Table V.

For the purpose of comparison with the theory, the enhancements of the integrated absorption coefficients can be represented as

$$c\int \tilde{\alpha}_{en}(\nu)d\nu = \tilde{\alpha}_{1b}\tilde{\rho}_a\tilde{\rho}_b + \tilde{\alpha}_{2b}\tilde{\rho}_a\tilde{\rho}_b^2 + \cdots\cdots \quad , \tag{3-2}$$

where c is the speed of light, $\tilde{\alpha}_{en}(\nu) = \alpha_{en}(\nu)/\nu$ is the enhancement in the absorption coefficient at a frequency ν with the frequency factor removed, and $\tilde{\rho}_a$ and $\tilde{\rho}_b$ are the number densities (number of molecules per unit volume) of the absorbing and perturbing gases, respectively. The relations between the quantities in eq. (3-1) and the corresponding quantities in eq. (3-2) are

$$\tilde{\rho}_a = \rho_a n_o \quad , \qquad \tilde{\rho}_b = \rho_b n_o \quad , \tag{3-3}$$

TABLE III

ENHANCEMENTS OF THE INTEGRATED ABSORPTION COEFFICIENTS OF THE FUNDAMENTAL BAND OF HYDROGEN IN H_2-He MIXTURES

Temperature (^oK)	ρ_{H_2} (amagat)	ρ_{He} (amagat)	$\int\alpha_{en}(\nu)d\nu$ (cm^{-2})	$(1/\rho_a\rho_b)\int\alpha_{en}(\nu)d\nu$ (10^{-3} cm^{-2} $amagat^{-2}$)
298	11.6	19	0.43	2.0
		54	1.15	1.83
		71	1.55	1.89
		88	1.83	1.80
		104	2.25	1.86
		121	2.55	1.82
		136	2.90	1.84
		154	3.29	1.84
	18.7	19	0.73	2.08
		34	1.38	2.16
		51	1.91	1.99
		66	2.41	1.96
		79	2.94	1.98
		93	3.46	1.98
		109	4.00	1.97
		122	4.36	1.92
		138	4.96	1.92

TABLE III, continued

Temperature (^{o}K)	ρ_{H_2} (amagat)	ρ_{He} (amagat)	$\int \alpha_{en}(\nu)d\nu$ (cm^{-2})	$(1/\rho_a\rho_b)\int \alpha_{en}(\nu)d\nu$ (10^{-3} cm^{-2} $amagat^{-2}$)
298	19.3	35	1.60	2.38
		53	2.16	2.10
		70	2.74	2.04
		86	3.34	2.02
		101	3.83	1.97
		117	4.61	2.03
		135	5.17	1.99
273	12.4	43	0.85	1.6
		65	1.35	1.67
		87	1.77	1.65
		107	2.12	1.61
		126	2.58	1.66
		148	3.06	1.67
		164	3.43	1.70
		183	3.84	1.70
		203	4.40	1.76
	13.1	21	0.42	1.6
		40	0.83	1.6
		51	1.04	1.55
		70	1.51	1.66
		85	1.84	1.66

TABLE III, continued

Temperature (^{o}K)	ρ_{H_2} (amagat)	ρ_{He} (amagat)	$\int\alpha_{en}(\nu)d\nu$ (cm^{-2})	$(1/\rho_a\rho_b)\int\alpha_{en}(\nu)d\nu$ (10^{-3} cm^{-2} $amagat^{-2}$)
273	13.1	102	2.24	1.68
		116	2.56	1.69
		131	2.93	1.71
		147	3.29	1.71
		174	4.00	1.75
		189	4.36	1.76
		202	4.68	1.77
		217	5.09	1.79
		232	5.48	1.81
	14.7	20	0.49	1.7
		39	0.96	1.7
		58	1.36	1.59
		76	1.79	1.60
		99	2.30	1.58
		112	2.79	1.69
		130	3.17	1.67
		146	3.62	1.69
		163	4.15	1.73
	15.5	42	1.16	1.78
		60	1.62	1.73
		78	2.11	1.74

TABLE III, continued

Temperature (^{o}K)	ρ_{H_2} (amagat)	ρ_{He} (amagat)	$\int\alpha_{en}(\nu)d\nu$ (cm^{-2})	$(1/\rho_a\rho_b)\int\alpha_{en}(\nu)d\nu$ (10^{-3} cm^{-2} $amagat^{-2}$)
273	15.5	96	2.59	1.74
		114	3.06	1.72
		131	3.51	1.73
		148	3.89	1.70
195	14.4	34	0.73	1.5
		60	1.18	1.38
		86	1.64	1.32
		111	2.03	1.27
		135	2.43	1.25
		161	3.01	1.30
		184	3.26	1.23
		207	3.85	1.27
	15.6	33	0.69	1.4
		58	1.28	1.41
		85	1.71	1.29
		110	2.20	1.28
		134	2.64	1.27
		159	3.17	1.28
		182	3.58	1.26
		205	4.04	1.26

TABLE III, continued

Temperature (^{o}K)	ρ_{H_2} (amagat)	ρ_{He} (amagat)	$\int\alpha_{en}(\nu)d\nu$ (cm^{-2})	$(1/\rho_a\rho_b)\int\alpha_{en}(\nu)d\nu$ (10^{-3} cm^{-2} $amagat^{-2}$)
77	57.5	57	1.8*	0.55
		119	3.5	0.52
		116	4.8	0.51
		223	7.4	0.57
		268	8.4	0.54
		321	10.6	0.58
		368	11.4	0.54
	59.3	104	3.3	0.54
		186	5.4	0.49
		257	7.8	0.52
		312	9.8	0.53
		353	11.6	0.56
		411	13.6	0.56
		500	15.4	0.58

*The values of $\int\alpha_{en}(\nu)d\nu$ for experiments at 77^{o}K are given correct to the first decimal place. This is because of the increased noise level in the traces, resulting from temperature fluctuations of the PbS detector in these experiments.

TABLE IV

ENHANCEMENTS OF THE INTEGRATED ABSORPTION COEFFICIENTS OF THE FUNDAMENTAL BAND OF HYDROGEN IN H_2-Ne MIXTURES

Temperature (^oK)	ρ_{H_2} (amagat)	ρ_{Ne} (amagat)	$\int\alpha_{en}(\nu)d\nu$ (cm^{-2})	$(1/\rho_a\rho_b)\int\alpha_{en}(\nu)d\nu$ (10^{-3} cm^{-2} $amagat^{-2}$)
298	13.0	9	0.29	2.5
		28	0.90	2.5
		36	1.14	2.45
		45	1.41	2.43
		53	1.65	2.42
		62	2.04	2.56
		82	2.62	2.49
	15.0	11	0.42	2.6
		19	0.74	2.6
		28	1.07	2.50
		38	1.47	2.57
		47	1.74	2.50
		55	2.07	2.51
		64	2.41	2.50
		71	2.70	2.52
		81	3.07	2.52
		89	3.39	2.55

TABLE IV, continued

Temperature (^{o}K)	ρ_{H_2} (amagat)	ρ_{Ne} (amagat)	$\int\alpha_{en}(\nu)d\nu$ (cm^{-2})	$(1/\rho_a\rho_b)\int\alpha_{en}(\nu)d\nu$ (10^{-3} cm^{-2} $amagat^{-2}$)
273	14.3	23	0.78	2.4
		34	1.12	2.31
		45	1.45	2.25
		57	1.84	2.25
		67	2.20	2.30
		76	2.44	2.25
		87	2.86	2.28
	14.1	14	0.42	2.2
		27	0.76	2.0
		40	1.17	2.08
		52	1.57	2.12
		65	2.03	2.21
		78	2.45	2.23
		89	2.85	2.27
		100	3.17	2.25
195	11.4	26	0.56	1.9
		48	1.05	1.93
		69	1.48	1.89
		93	2.01	1.90
		114	2.41	1.84
		136	2.90	1.87

TABLE IV, continued

Temperature (^{o}K)	ρ_{H_2} (amagat)	ρ_{Ne} (amagat)	$\int\alpha_{en}(\nu)d\nu$ (cm^{-2})	$(1/\rho_a\rho_b)\int\alpha_{en}(\nu)d\nu$ (10^{-3} cm^{-2} $amagat^{-2}$)
195	11.4	155	3.31	1.87
		176	3.67	1.83
	13.8	20	0.50	1.8
		41	1.08	1.89
		61	1.65	1.95
		80	2.00	1.82
		97	2.31	1.72
		117	2.79	1.73
		134	3.23	1.75
		149	3.48	1.70
77	28.1	125	3.0*	0.85
		222	5.1	0.83
		308	6.9	0.80
		382	9.9	0.92
		446	10.9	0.87
		503	12.2	0.89
	33.7	53	1.9	1.04
		114	3.4	0.89
		198	6.9	1.03

TABLE IV, continued

Temperature (^{o}K)	ρ_{H_2} (amagat)	ρ_{Ne} (amagat)	$\int\alpha_{en}(\nu)d\nu$ (cm^{-2})	$(1/\rho_a\rho_b)\int\alpha_{en}(\nu)d\nu$ (10^{-3} cm^{-2} $amagat^{-2}$)
77	33.7	262	8.5	0.97
		323	11.2	1.03
		378	13.1	1.03
		443	15.6	1.04
		493	16.9	1.02
	36.2	109	4.0	1.02
		188	6.0	0.88
		267	9.0	0.93
		334	10.6	0.88
		380	12.6	0.92
		445	13.8	0.86

* Same as the footnote in Table III.

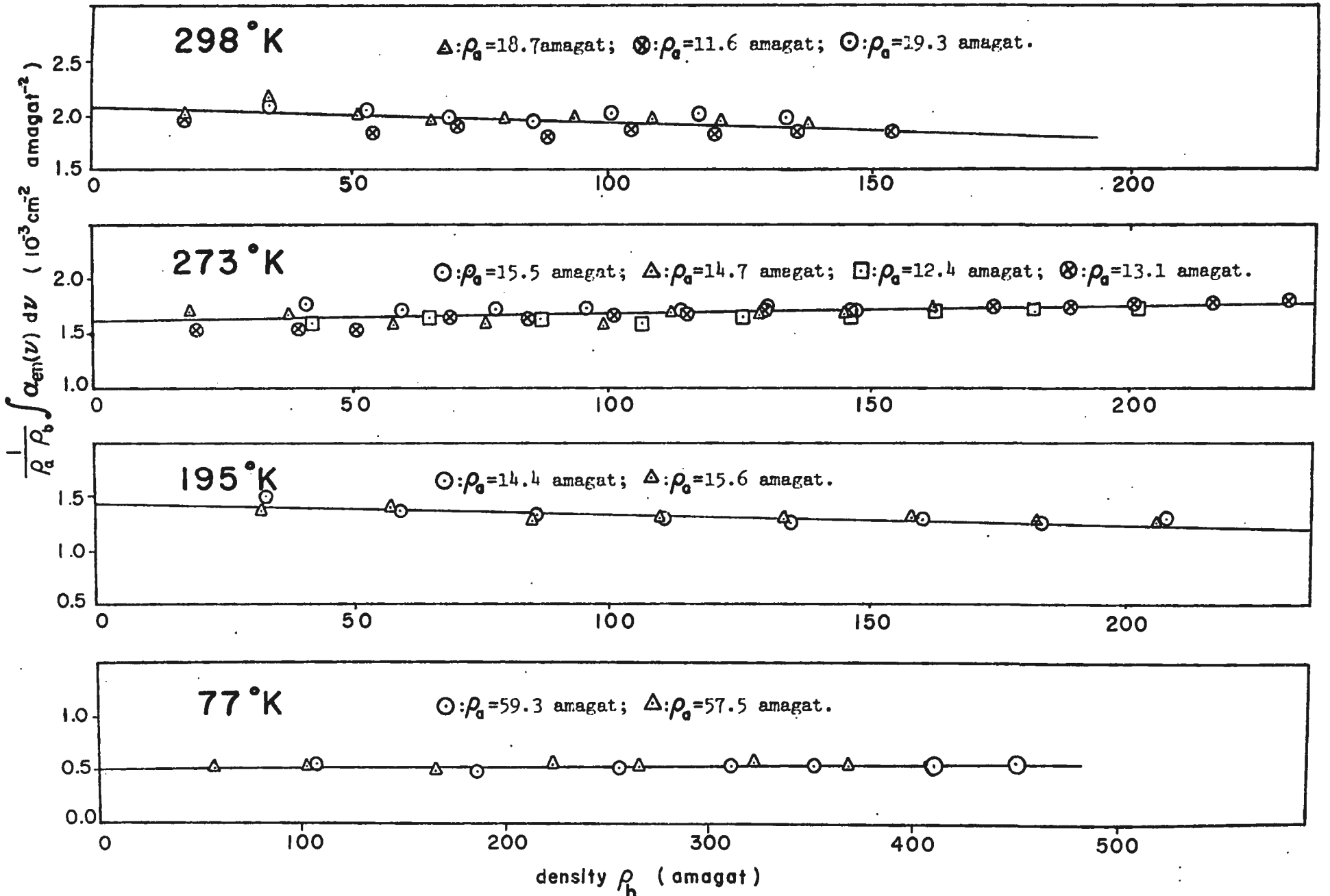

Fig.17. The relation between the enhancements in the integrated absorption coefficients of the fundamental band of hydrogen and ρ_a and ρ_b in H_2-He mixtures at 298°K, 273°K, 195°K and 77°K.

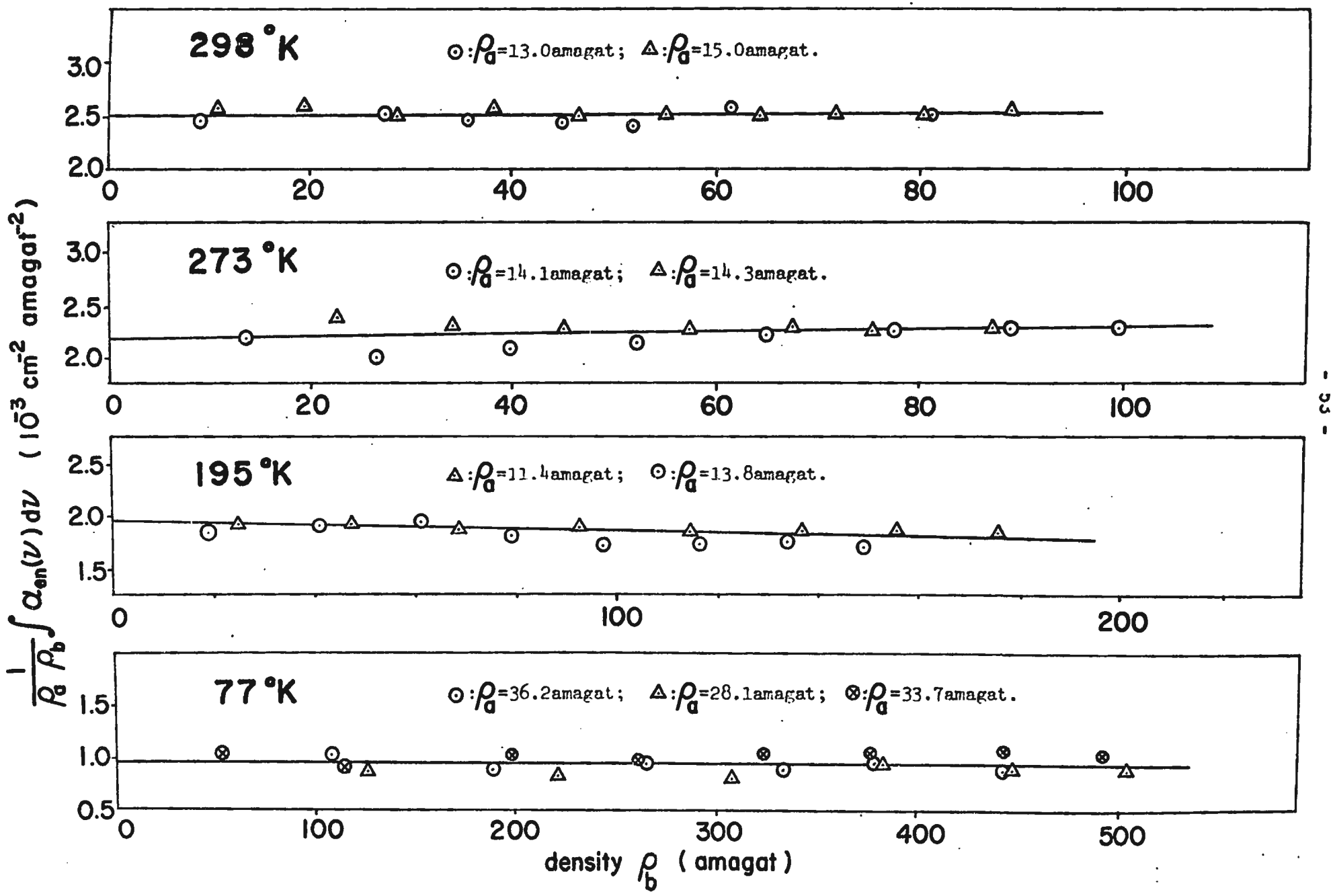

Fig.18. The relation between the enhancements in the integrated absorption coefficients of the fundamental band of hydrogen and ρ_a and ρ_b in H_2-Ne mixtures at 298°K, 273°K, 195°K and 77°K.

TABLE V

ABSORPTION COEFFICIENTS OF THE INDUCED FUNDAMENTAL BAND OF HYDROGEN IN H_2-He AND H_2-Ne MIXTURES

Mixture	Temperature (^oK)	Binary absorption coefficient α_{1b} (10^{-3} cm^{-2} amagat^{-2})	Binary absorption coefficient $\tilde{\alpha}_{1b}$ (10^{-35} cm^6 s^{-1})	Ternary absorption coefficient α_{2b} (10^{-6} cm^{-2} amagat^{-3})
H_2-He	298	2.08 ± 0.06	1.99 ± 0.06	-1.40 ± 0.64
	273	1.61 ± 0.02	1.54 ± 0.02	0.61 ± 0.15
	195	1.43 ± 0.03	1.36 ± 0.03	-0.96 ± 0.22
	77	0.51 ± 0.02	0.49 ± 0.02	0.11 ± 0.05
H_2-Ne	298	2.51 ± 0.03	2.40 ± 0.03	0.02 ± 0.52
	273	2.16 ± 0.06	2.07 ± 0.06	1.07 ± 0.99
	195	1.92 ± 0.04	1.82 ± 0.04	-0.81 ± 0.37
	77	0.94 ± 0.05	0.89 ± 0.05	-0.03 ± 0.14

(3-4) $$\tilde{\alpha}_{1b} = (c/n_o^2)\alpha_{1b}/\bar{\nu} \quad , \qquad \tilde{\alpha}_{2b} = (c/n_o^3)\alpha_{2b}/\bar{\nu}$$

where n_o is Loschmidt's number (number density of an ideal gas at S.T.P.: 2.687×10^{19} cm^{-3}) and $\bar{\nu}$ is the centre of the band which is given by

(3 5) $$\bar{\nu} = \int \alpha_{en}(\nu)d\nu / \int \nu^{-1}\alpha_{en}(\nu)d\nu \quad .$$

The new binary and ternary coefficients $\tilde{\alpha}_{1b}$ and $\tilde{\alpha}_{2b}$ represent the transition probabilities induced in collisions of types a-b and b-a-b, respectively. The average values of $\bar{\nu}$ for H_2-He and H_2-Ne at 298^oK, 273^oK, 195^oK and 77^oK are 4335 cm^{-1}, 4388 cm^{-1}, 4354 cm^{-1} and 4373 cm^{-1}, respectively. The values of $\tilde{\alpha}_{1b}$ (cm^6 s^{-1}) for H_2-He and H_2-Ne are also included in Table V. Finally the values of the binary absorption coefficients of the collision-induced fundamental band of hydrogen in H_2-He and H_2-Ne obtained by different researchers are compared in Table VI.

The values of the binary absorption coefficients in H_2-He at 298^oK and 195^oK obtained in the present work are considerably higher, and that at 77^oK is considerably lower than the values obtained by earlier researchers. To check the consistency of the experimental results of the present work, we measured the absorption of the induced fundamental band of H_2 in the pure gas at room temperature and obtained a value of $(2.44 \pm 0.02) \times 10^{-3}$ cm^{-2} $amagat^{-2}$ for the binary absorption coefficient which was in close agreement with the values, 2.5×10^{-3}, 2.4×10^{-3} and 2.42×10^{-3} cm^{-2} $amagat^{-2}$, obtained respectively by Chisholm and Welsh (1954), Hare and Welsh (1958) and Hunt (1959). The discrepancy between the values obtained in the present work and those obtained by the earlier

TABLE VI

COMPARISON OF THE BINARY ABSORPTION COEFFICIENTS OF THE H_2 FUNDAMENTAL BAND IN H_2-He AND H_2-Ne MIXTURES

Mixture	Temperature (^oK)	α_{1b} (10^{-3} cm^{-2} $amagat^{-2}$)	Reference
H_2-He	298	1.5	Chisholm and Welsh (1954)
	298	1.1	Hare and Welsh (1958)
	300	1.57	Hunt (1959)
	298	2.08	Present work
	273	1.61	Present work
	200	1.3	Chisholm and Welsh (1954)
	195	0.93	Hunt (1959)
	195	1.43	Present work
	85	0.75	Hunt (1959)
	77	0.51	Present work
H_2-Ne	298	2.50	Reddy and Lee (1968)
	298	2.51	Present work
	273	2.16	Present work
	195	1.92	Present work
	77	0.94	Present work

researchers for H_2-He may be attributed to the following facts: the earlier researchers might have experienced considerable uncertainty in determining the absorption in the wings of the spectra, and the values given by them were obtained from measurements at relatively much higher pressures than those in the present work.

3.3 Discussion

In the spectra of collision-induced absorption, the overlap as well as the quadrupolar components are modulated by the translational motion of the colliding pairs of molecules. Hence, the frequency distribution of each component of the fundamental band can be represented as the summation and difference tones, $\nu_m(J) \pm \nu_{tr}$, where $\nu_m(J)$ is the molecular frequency of the transition and ν_{tr} is the continuum of frequencies corresponding to all possible values of the relative translational energy of the colliding pairs of molecules (see, for example, Watanabe and Welsh,1967). The experimentally observed splitting of the Q branch into Q_P and Q_R is considered to be the result of the splitting of the individual components ($Q_{overlap}(J)$) of the overlap part of the Q branch, with their minima occurring at the corresponding molecular frequencies $\nu_m(J)$. The occurrence of the dip was shown by Van Kranendonk (1968) to be an interference effect due to correlations existing between the overlap dipole moments in successive collisions. The splitting of the S(0) and S(1) lines in H_2-He and H_2-Ne mixtures into S_P and S_R components indicates that there is a considerable amount of contribution of the anisotropy of the overlap moment to the intensity of the so-called 'quadrupolar' S(0) and S(1) lines.

3.4 Errors in the Estimated Values of the Binary Absorption Coefficients

In section 3.2 the binary absorption coefficients were obtained from the intercepts of the straight line fits of $(1/\rho_a\rho_b)\int\alpha_{en}(\nu)d\nu$ against ρ_b. To obtain these fits a large number of data (in some cases as large as 39 determinations) were used for a binary mixture at a given temperature. For example, the binary absorption coefficient for H_2-He at 298^oK was obtained from 23 determinations and its value is

$$\alpha_{1b} = (2.08 \pm 0.06) \times 10^{-3} \text{ cm}^{-2} \text{ amagat}^{-2} \quad .$$

Here, the probable error ± 0.06 corresponds to ± 3%, approximately. The probable errors in the values of the binary absorption coefficients could have been caused by a number of random errors, the most obvious of which are:

(i) error in the measurement of the gas pressures,

(ii) error in matching the background absorption traces due to random changes in the source characteristics,

(iii) error in matching the background absorption traces due to random changes in the detector and amplifier characteristics,

(iv) error in the measurement of $\log_{10}(I_1/I_2)$ from the recorder traces.

In the measurement of gas pressures, 7 different gauges with maximum readings in the range 160 p.s.i. to 10,000 p.s.i. were used. These gauges were calibrated against standard gauges which were, in turn, calibrated carefully against a dead weight test gauge. The accuracies claimed in the readings for the 160 p.s.i. and 10,000 p.s.i. gauges, for

example, are ± 1 p.s.i. and ± 50 p.s.i., respectively. The corresponding fractional errors for a reading of 100 p.s.i. on the first gauge and for a reading of 5,000 p.s.i. on the second gauge are ± 1%.

The source used was a very stable water-cooled 750-watt projection lamp which was operated at a lower voltage than its rated value and by feeding the same from a stabilized power supply unit. The stability of the source has been verified by taking background traces before and after each set of experiments.

The temperature variation of the PbS detector causes its sensitivity to vary. Precautions were taken to maintain the temperature of the detector steady throughout the experiments. However, for the experiments at $77^{o}K$, the temperature of the detector was found to fluctuate appreciably because of the nearness of the detector to the absorption cell which was cooled in a liquid nitrogen bath. The greater probable errors in α_{1b} for H_2-He and H_2-Ne at $77^{o}K$, which are 4% and 5%, respectively, may be attributed largely to this effect.

The fractional errors in the measurement of $\log_{10}(I_1/I_2)$ of the enhancement absorption profiles are, in general, large or small depending on whether the total enhancement absorption measured is small or large, respectively. The estimated fractional errors in the integrated absorption coefficients are approximately of the order of 2% and 12%.

In addition to the random errors discussed above there may be a systematic error caused by the inaccuracy in establishing the infinite absorption line. This error was minimized by checking the infinite absorption line at several intervals during an experiment.

CHAPTER 4

OVERLAP PARAMETERS OF THE COLLIDING PAIRS H_2-He AND H_2-Ne

4.1 Theoretical Expressions Applicable to the Experimental Results

According to the theory of the collision-induced fundamental infrared absorption band of symmetric diatomic gases (see Appendix A), the binary absorption coefficient $\tilde{\alpha}_{1b}$ of a binary mixture of a symmetric diatomic gas with a monatomic perturbing gas (zero quadrupole moment) can be expressed as a sum of two terms, one term ($\lambda^2 \mathbf{I}\,\tilde{\gamma}$) due to the contribution from short-range electron overlap interaction and the other ($(Q_1'\alpha_2/e\sigma^4)^2 \mathbf{J}\,\tilde{\gamma}$) due to a long-range quadrupolar induction. Thus,

$$\tilde{\alpha}_{1b} = \lambda^2 \mathbf{I}\,\tilde{\gamma} + \left[\frac{Q_1'\alpha_2}{e\sigma^4}\right]^2 \mathbf{J}\,\tilde{\gamma} \quad . \tag{4-1}$$

Here the dimensionless overlap parameter λ is given by

$$\lambda = (\xi/e)\,\exp(-\sigma/\rho) \quad , \tag{4-2}$$

ξ and ρ being the strength of the short-range overlap induced dipole moment and its range, respectively. σ is the Lennard-Jones intermolecular diameter for a pair of colliding molecules 1 and 2, and e is the absolute value of the electronic charge. $\tilde{\gamma}$ is given by

$$\tilde{\gamma} = \kappa e^2\sigma^3 = \pi e^2\sigma^3/3m_o\nu_o \tag{4-3}$$

where m_o and ν_o are the reduced mass and the frequency of oscillation (in s^{-1}) respectively of the absorbing molecule. Q_1' is the derivative of the quadrupole moment of molecule 1 with respect to its internuclear distance at its equilibrium value and α_2 is the average polarizability of molecule 2. The dimensionless definite integrals

$$I = 4\pi \int_0^\infty \exp(-2(x-1)\sigma/\rho)\, g_o(x)\, x^2 dx \tag{4-4}$$

and

$$J = 12\pi \int_0^\infty x^{-8}\, g_o(x)\, x^2 dx \tag{4-5}$$

where $x = R^* = R/\sigma$, R being the intermolecular separation and $g_o(x)$ is the low density limit of the pair distribution function. At higher temperatures, $g_o(x)$ is equal to the classical value, $\exp(-V(x)/kT)$. At intermediate temperatures, $g_o(x)$ may be expanded as an asymptotic series in powers of Planck's constant (de Boer 1949). The resulting expressions for I and J are

$$I = I_{cl} - \Lambda^{*2} I^{(2)} + \Lambda^{*4} I^{(4)} + \cdots \tag{4-6}$$

and

$$J = J_{cl} - \Lambda^{*2} J^{(2)} + \Lambda^{*4} J^{(4)} + \cdots \tag{4-7}$$

where $I^{(2)}$, $I^{(4)}$, $J^{(2)}$ and $J^{(4)}$ are the quantum corrections, and

$$\Lambda^* = (h^2/2m_{oo}\varepsilon\sigma^2)^{\frac{1}{2}} \tag{4-8}$$

is the reduced mean de Broglie wavelength, m_{oo} being the reduced mass of the colliding pair of molecules, h is Planck's constant, ε is the depth of Lennard-Jones potential.

At lower temperatures the pair distribution function $g_o(x)$ may be calculated entirely quantum-mechanically from the radial wavefunction of the two colliding molecules. Poll (1960) has made such calculations of the pair distribution function for H_2-H_2 collisions by expressing the function in terms of the solutions of the Schroedinger equation for the relative motion of the two molecules. His calculations have shown that a pair of H_2 molecules has two bound states corresponding to the rotation of the complex $(H_2)_2$. At lower temperatures the binary absorption coefficient may be thought of as arising from two contributions, one from the bound states and the other from the scattering states. These two contributions differ greatly in their temperature dependence. The contribution from the bound states increases with decreasing temperature because the number of bound molecules increases. On the other hand, the contribution from the scattering states decreases with decreasing temperature because the distance of closest approach of the molecules becomes greater. Poll's calculations have also shown that the contribution from the bound states of the $(H_2)_2$ complexes causes the binary absorption coefficient to increase at temperatures below 40^oK. Watanabe and Welsh (1964; 1965) did, in fact, observe at temperatures below 40^oK, not only an increase in the binary absorption coefficient of the pure hydrogen gas but also fine structures in the Q and S branches of its absorption profiles, which are characteristic of the bound states of the $(H_2)_2$ complexes. These authors (1965) also studied the absorption of H_2-He mixtures at 20.0^oK in the H_2 fundamental region but could not observe any bound states, nor did they observe any increase in the binary absorption coefficient. The absence of the bound states for a H_2-He pair was

explained by these authors as due to the smaller depth (ε) of the Lennard-Jones potential for H_2-He (for H_2-He, ε/k = 19.45°K compared to 37.0°K for H_2-H_2 pairs). Since the present work concerns the binary mixtures H_2-He and H_2-Ne (ε/k = 36.29°K) at temperatures above 77°K, we did not attempt to calculate the pair distribution functions for these mixtures entirely quantum-mechanically.

4.2 Calculation of the Quadrupolar Parts ($\tilde{\alpha}_{1b}^{quad}$) of the Binary Absorption Coefficients

Recent theoretical calculations of Karl and Poll (1967) and Birnbaum and Poll (1969) indicate that the matrix elements of the quadrupole moment between different vibrational states of hydrogen, $< vJ \mid Q \mid v'J' >$, are sensitive to the values of J and J' (see Appendix B). Consequently, Q' in eq. (4-1) is no longer a constant. Its values for different transitions in the fundamental band of hydrogen are given by the approximate relation

$$Q' = \frac{1}{r_e(B/\omega)^{\frac{1}{2}}} < 0J \mid Q \mid 1J' > \quad . \tag{4-9}$$

The value of the matrix elements $< 0J \mid Q \mid 1J' >$ for the O, Q and S lines are obtained from Birnbaum and Poll (1969) and are listed in Table B-2 of Appendix B. For the hydrogen molecule, r_e = 1.40108 a_o, B = 60.9 cm^{-1} and ω = 4162 cm^{-1}. The values of Q' for different transitions of the fundamental band of hydrogen are listed in Table VII.

TABLE VII

VALUE OF Q' FOR THE HYDROGEN MOLECULE (IN UNITS OF ea_o)

	O lines	Q lines	S lines
J	$\frac{1}{r_e(B/\omega)^{\frac{1}{2}}} \langle 0J\|Q\|1J-2\rangle$	$\frac{1}{r_e(B/\omega)^{\frac{1}{2}}} \langle 0J\|Q\|1J\rangle$	$\frac{1}{r_e(B/\omega)^{\frac{1}{2}}} \langle 0J\|Q\|1J+2\rangle$
0		0.5188	0.4623
1		0.5192	0.4252
2	0.5761	0.5201	0.3886
3	0.6143	0.5214	0.3525

Since Q' is different for different transitions of the fundamental band of hydrogen, the binary absorption coefficients of the individual quadrupolar components were calculated first and the total quadrupolar binary absorption coefficient $\bar{\alpha}_{1b}^{quad}$ was then obtained from their sum. The details of the calculations are given below. The molecular parameter used in the calculations are listed in Table VIII. Values of the depth of the Lennard-Jones potential and those of the Lennard-Jones diameter σ were taken from Hirschfelder, Curtiss and Bird (1967). For the mixtures, the geometric mean of the values of ϵ and the arithmetic mean of the values of σ of the component gases were taken. The de Broglie wavelengths Λ^* were calculated using eq. (4-8). The integral J at different reduced temperatures T^* ($=kT/\epsilon$) up to a value of 10 were taken from Van Kranendonk and Kiss (1959). For T^* greater

TABLE VIII

MOLECULAR CONSTANTS FOR H_2-He AND H_2-Ne MIXTURES

Mixture	T (^oK)	ε/k (^oK)	σ (Å)	T*	$\tilde{\gamma}$ (10^{-32} cm^6 s^{-1})	α_2/a_o^3 (for perturber)	Λ^*	J.
H_2-He	298	19.37	2.757	15.3	4.772	1.4	2.215	15.27
"	273	"	"	14.0	"			14.78
"	195	"	"	10.0	"			13.48
"	77	"	"	3.96	"			11.22
H_2-Ne	298	36.15	2.854	8.21	5.293	2.7	1.337	13.15
"	273	"	"	7.52	"			12.91
"	195	"	"	5.37	"			12.10
"	77	"	"	2.12	"			11.50

than 10, J_{cl} was evaluated using a computer program on IBM 360. In calculating J, the quantum corrections $J^{(2)}$ and $J^{(4)}$ mentioned in eq. (4-7) were applied to the classical values of J_{cl}. The polarizabilities, α_2, of helium and neon were taken from Hirschfelder, Curtiss and Bird (1967).

The values of the binary absorption coefficients of the individual quadrupolar components of the fundamental band of hydrogen were obtained from the expression

$$(4\text{-}10) \qquad \tilde{\alpha}_{1b}^{quad}(B(J)) = \left[\frac{(1/r_e(B/\omega)^{\frac{1}{2}}) < 0J \mid Q \mid 1J' >}{e\sigma^4}\alpha_2\right]^2 P(J)L_2(J,J')J\tilde{\gamma} \quad .$$

Here

$$(4\text{-}11) \qquad P(J) = \frac{g_T \exp(-J(J+1)B_0\, hc/kT)}{\sum_J g_T g_J \exp(-J(J+1)B_0\, hc/kT)}$$

are the normalized Boltzmann factors, normalized in terms of the Racah coefficients $L_2(J,J')$ such that

$$\sum_J (2J+1)P(J) = 1 \quad ,$$

and $g_T(= 2T + 1)$ is the degeneracy due to nuclear spin and $g_J = (2J + 1)$ is the degeneracy of the rotational state J. For the O(J), Q(J) and S(J), the Racah coefficients $L_2(J,J')$ are $L_2(J,J-2)$, $L_2(J,J)$ and $L_2(J,J+2)$, respectively. Since the nuclear spin, I, of a hydrogen atom is ½, the total nuclear spin, T, of a hydrogen molecule takes values 1 (parallel spins) and, 0, (anti-parallel spins). Even T values are possible for symmetric levels (J = 0, 2, ...) and odd T values for antisymmetric

levels (J = 1, 3, ...). The nuclear statistical weight 2T + 1 is therefore 1 and 3 for the even and odd rotational levels, respectively. The values of P(J) for H_2 at the four experimental temperatures are summarized in Table IX. The sum $\sum_{J,B(J)} \tilde{\alpha}_{1b}(B(J))$ gives the total quadrupolar binary absorption coefficient $\tilde{\alpha}_{1b}^{quad}$. The calculated values of the binary absorption coefficients of the individual quadrupolar components together with those of $\tilde{\alpha}_{1b}^{quad}$ for H_2-He and H_2-Ne mixtures for all the experimental temperatures are summarized in Table X.

The experimental values of the binary absorption coefficients $\tilde{\alpha}_{1b}^{quad}$ in units of $cm^6\ s^{-1}$ (chapter 3) and the values of $\tilde{\alpha}_{1b}^{quad}$ calculated as described above are listed in Table XI. The overlap parts $\lambda^2 \mathbf{I}\tilde{\gamma}$ were obtained by subtracting $\tilde{\alpha}_{1b}^{quad}$ from the corresponding $\tilde{\alpha}_{1b}$ and are given in the same table. The percentage contributions of the quadrupolar and overlap parts to the binary absorption coefficient are also listed in the same table. It is seen that in the temperature range 77^oK to 298^oK the overlap parts contribute 91 to 97% for H_2-He mixtures and 84 to 93% for H_2-Ne mixtures.

4.3 Determination of the Overlap Parameters for H_2-He and H_2-Ne Pairs

Using the values of $\tilde{\gamma}$ given in Table VIII, the values of $\lambda^2 \mathbf{I}$ for H_2-He and H_2-Ne were obtained and are given in Table XII. These were plotted against temperature T in Figs. 19 and 20, respectively. The integral $\mathbf{I}$ given by eq. (4-4) depends on the factor σ/ρ, the ratio of the Lennard-Jones diameter of a colliding pair of molecules and the range of the overlap moment. A study of the variation of $\lambda^2 \mathbf{I}$ in H_2-He and H_2-Ne mixtures as a function of temperature enables us to determine

TABLE IX

NORMALIZED BOLTZMANN FACTORS FOR HYDROGEN AT DIFFERENT TEMPERATURES

	P(J)			
J	298°K	273°K	195°K	77°K
0	0.1338	0.1447	0.1962	0.5182
1	0.2230	0.2284	0.2396	0.1597
2	0.0229	0.0211	0.0132	0.0006
3	0.0118	0.0092	0.0027	0.0000
—	———	———	———	———
$\Sigma(2J+1)P(J)$	0.9999	0.9998	0.9999	1.0003

TABLE X

BINARY ABSORPTION COEFFICIENTS OF THE INDIVIDUAL QUADRUPOLAR COMPONENTS (IN UNITS OF 10^{-35} cm^6 s^{-1})

Mixture	Temperature (^oK)	O(3)	O(2)	Q(1)	Q(2)	Q(3)	S(0)	S(1)	S(2)	S(3)	Total quadrupolar binary absorption coefficient $\tilde{\alpha}_{1b}^{quad}$
H_2-He	298	0.002	0.002	0.020	0.002	0.002	0.008	0.020	0.002	0.001	0.060
"	273	0.002	0.002	0.020	0.002	0.001	0.008	0.020	0.002	0.001	0.059
"	195	—	0.001	0.019	0.001	—	0.010	0.019	0.001	—	0.053
"	77	—	—	0.010	—	—	0.022	0.010	—	—	0.044
H_2-Ne	298	0.006	0.006	0.053	0.007	0.004	0.021	0.054	0.007	0.004	0.164
"	273	0.005	0.005	0.054	0.006	0.003	0.023	0.054	0.006	0.003	0.160
"	195	0.001	0.003	0.053	0.003	0.001	0.029	0.053	0.004	0.001	0.149
"	77	—	—	0.033	—	—	0.072	0.034	—	—	0.139

TABLE XI

QUADRUPOLAR AND OVERLAP PARTS OF THE BINARY ABSORPTION COEFFICIENTS

Mixture	Temperature (^{o}K)	Binary absorption coefficient (10^{-35} cm^6 s^{-1})	Quadrupolar part (10^{-35} cm^6 s^{-1})	Overlap part (10^{-35} cm^6 s^{-1})	Percentage Quad.	Percentage Overlap
H_2-He	298	1.99	0.06	1.93	3.0	97.0
"	273	1.54	0.06	1.48	3.9	96.1
"	195	1.36	0.05	1.31	3.9	96.1
"	77	0.49	0.04	0.45	9.1	90.9
H_2-Ne	298	2.40	0.16	2.24	6.7	93.3
"	273	2.07	0.16	1.91	7.7	92.3
"	195	1.82	0.15	1.67	8.2	91.8
"	77	0.89	0.14	0.75	15.7	84.3

TABLE XII

VALUES OF $\mathbf{I}$ USED IN FITTING THE CALCULATED AND OBSERVED VALUES OF $\lambda^2\mathbf{I}$ AS A FUNCTION OF TEMPERATURE

Mixture	Temperature (^oK)	Observed $\lambda^2\mathbf{I}$ (10^{-4})	T*	Calculated $\mathbf{I}$	λ^2 (10^{-6})
H_2-He	298	4.045	15.33	12.57	31.0
"	273	3.105	14.04	11.42	"
"	195	2.738	10.03	7.97	"
"	77	0.9337	3.960	3.26	"
H_2-Ne	298	4.232	8.211	5.20	81.4
"	273	3.608	7.522	4.82	"
"	195	3.500	5.373	3.66	"
"	77	1.412	2.122	2.02	"

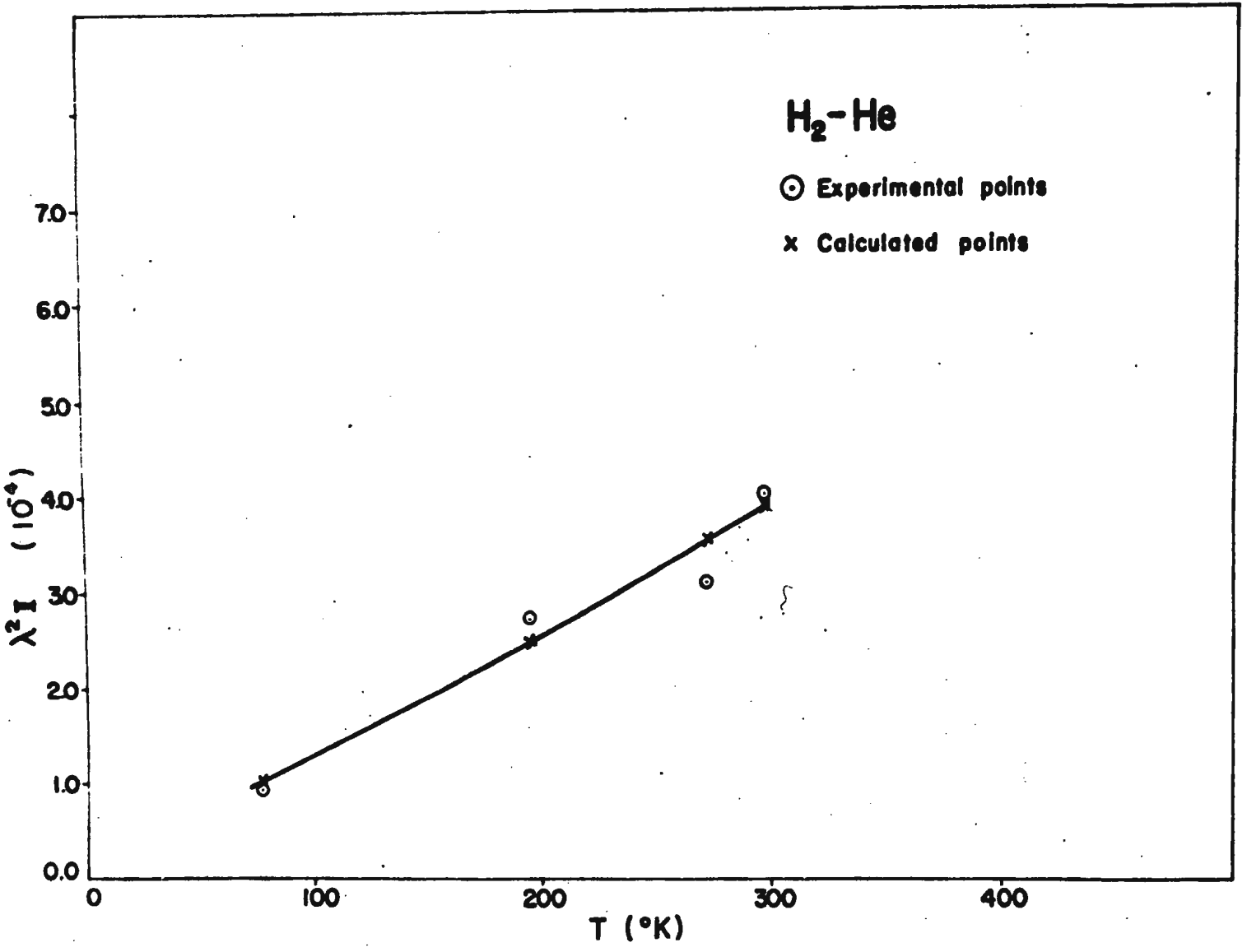

Fig. 19. Variation of $\lambda^2 I$ with the temperature for H_2 - He mixtures.

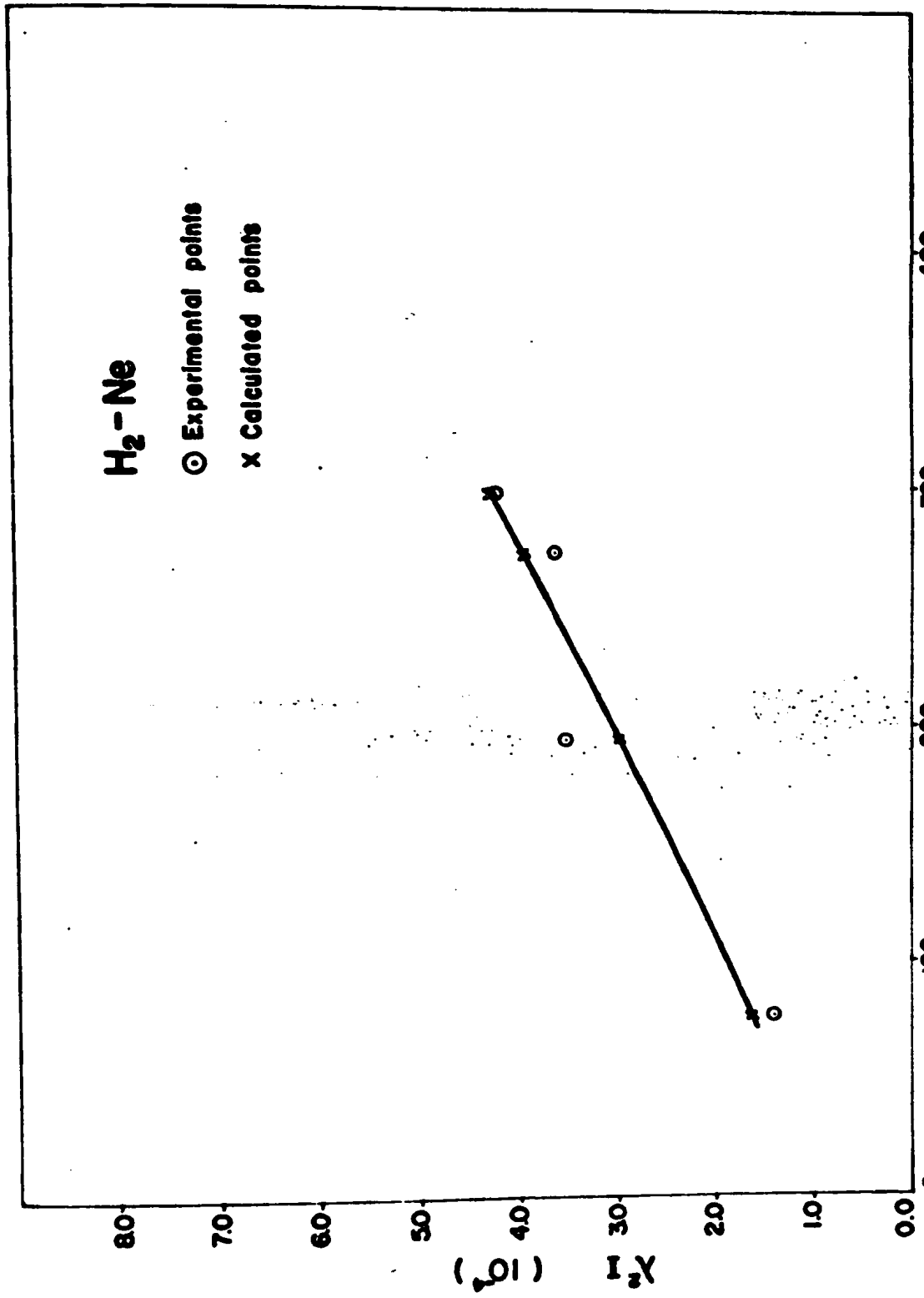

Fig.20. Variation of $\chi^2 I$ with the temperature for H_2-Ne mixtures.

the most probable values of σ/ρ for these mixtures. In order to determine the value of ρ/σ for each of the mixtures the following procedure was adopted. The values of I_{cl} were calculated from eq. (4-4) using a computer program written for the IBM 360 computer for a series of values of ρ/σ in the range 0.080 to 0.140 at intervals of 0.002 at reduced temperatures T* in the range 0.5 to 20.0 at intervals of 0.5. To obtain appropriate values of I, quantum corrections $I^{(2)}$ and $I^{(4)}$ were applied (eq. 4-6). These quantum corrections were either directly obtained or extrapolated from the data given by Van Kranendonk and Kiss (1959). For one particular value of ρ/σ, λ was calculated from $\lambda^2 I$ at one of the experimental temperatures using the corresponding value of I. Assuming that λ^2 is independent of temperature, $\lambda^2 I$ were calculated at the other three experimental temperatures. This procedure was repeated until the calculated values of $\lambda^2 I$ at all the experimental temperatures agreed closely with the observed values. The criterion for the best fit of the curve between $\lambda^2 I$ and T was that the sum of the squares of the deviations of the calculated values of $\lambda^2 I$ from the corresponding observed values be a minimum. The temperature dependence of the experimental and calculated values of $\lambda^2 I$ is shown for H_2-He and H_2-Ne in Figs. 19 and 20, respectively. The values of σ/ρ, ρ and λ for H_2-He and H_2-Ne evaluated in the present work are also given in Table XIII. For the purpose of comparison the values of ρ/σ and ρ for H_2-He obtained by Sears (1968a), and for He-Ar and Ne-Ar obtained by Sears (1968b) using the force auto correlation functions are also included in the same table. For H_2-He the values of these parameters obtained in the present work are in excellent agreement with those by Sears.

TABLE XIII

COMPARISON OVERLAP PARAMETERS FOR VARIOUS GAS MIXTURES

Mixture	ρ/σ	λ	σ (Å)	ρ (Å)	References
H_2-He	0.088	5.6×10^{-3}	2.757	0.24	Present thesis
H_2-Ne	0.100	9.0×10^{-3}	2.854	0.29	Present thesis
H_2-He	0.126				Van Kranendonk and Kiss (1959)
H_2-He	0.087		2.75	0.24	Sears (1968a)
He-Ar	0.110		3.0	0.33	Sears (1968b)
Ne-Ar	0.092		3.1	0.29	Sears (1968b)

The overlap radial integrals I_{c1} for $\sigma/\rho = 0.088$ (for H_2-He) and 0.100 (for H_2-Ne) for temperatures $T^* = 0.5$ to 20.0 are listed in Table XIV.

A word must be said on the error involved in calculating the quadrupolar part of the binary absorption coefficients using the molecular parameters of the colliding pair of the molecules. The major error lies in the uncertainty of the values of σ of the colliding pairs since it occurs in the 5th power in the expression for the binary absorption coefficient (see eq.(4-1)).

The numerical calculations have shown that the quadrupolar part of the binary absorption coefficients varies from 3% for H_2-He at 298^oK to 16% for H_2-Ne at 77^oK. For the sake of argument, even if one assumes an uncertainty as large as 25% in the calculation of quadrupolar parts, the percentage error in the overlap parts will not be very high; these are less than 1% for H_2-He at 298^oK and about 5% for H_2-Ne at 77^oK.

Another method of estimating the quadrupolar and overlap part of the binary absorption coefficient for the given binary mixture is by the method of profile analysis (see, for example, Watánabe and Welsh 1967). In this method there is no need to use the molecular parameters of the component gases except the relative strengthsof the individual lines of the fundamental band of hydrogen. However, for the H_2-He and H_2-Ne mixtures, particularly at higher temperatures, even the method of profile analysis may not yield more accurate values of quadrupolar part because the contribution of the overlap parts extends almost to the entire region of the fundamental band.

TABLE XIV

CLASSICAL VALUE OF THE OVERLAP RADIAL INTEGRAL I

FOR ρ/σ = 0.08 AND 0.100

T*	I_{cl}	
	ρ/σ = 0.088 (for H_2-He)	ρ/σ = 0.100 (for H_2-Ne)
0.5	2.50	2.98
1.0	1.67	1.84
1.5	1.76	1.83
2.0	1.99	1.99
2.5	2.27	2.20
3.0	2.57	2.43
3.5	2.90	2.67
4.0	3.24	2.92
4.5	3.59	3.18
5.0	3.95	3.44
5.5	4.32	3.71
6.0	4.69	3.97
6.5	5.07	4.24
7.0	5.45	4.51
7.5	5.85	4.79
8.0	6.25	5.06
8.5	6.65	5.34
9.0	7.06	5.61
9.5	7.46	5.88
10.0	7.88	6.16
10.5	8.30	6.44
11.0	8.72	6.72

TABLE XIV , continued

T*	I_{cl}	
	ρ/σ = 0.088 (for H_2-He)	ρ/σ = 0.100 (for H_2-Ne)
11.5	9.15	7.00
12.0	9.58	7.28
12.5	10.01	7.56
13.0	10.45	7.84
13.5	10.88	8.12
14.0	11.32	8.40
14.5	11.77	8.68
15.0	12.21	8.96
15.5	12.67	9.25
16.0	13.12	9.53
16.5	13.57	9.81
17.0	14.03	10.10
17.5	14.49	10.38
18.0	14.95	10.66
18.5	15.42	10.95
19.0	15.87	11.23
19.5	16.34	11.50
20.0	16.81	11.79

APPENDIX A

THEORY OF COLLISION-INDUCED INFRARED ABSORPTION

The absorption coefficient per unit path length, $\alpha(\nu)$, at a frequency (cm^{-1}), is defined by Beer's law

(A-1) $$I(\nu) = I_0(\nu) \exp(-\alpha(\nu)\ell)$$

where $I(\nu)$ is the intensity transmitted by an absorption cell of sample path length ℓ, containing an absorbing (pure) gas, when radiation of intensity $I_0(\nu)$ is incident on the cell. The enhancement in the absorption coefficient per unit path length, due to the addition of a foreign gas into the cell containing the absorbing gas at a particular base density is given by

(A-2) $$I_2(\nu) = I_1(\nu) \exp(-\alpha_{en}(\nu)\ell)$$

where $I_1(\nu)$ is the intensity transmitted by the absorbing gas in the cell and $I_2(\nu)$ is the intensity transmitted by the cell with the binary mixture. We obtain from eqs. (A-1) and (A-2)

(A-3) $$\alpha(\nu) = (1/\ell) \ln(I_0/I_1)$$

and

$$\alpha_{en}(\nu) = (1/\ell) \ln(I_1/I_2) \quad .$$

The integrated absorption coefficient for the collision-induced bands of symmetric diatomic gases can be expressed in power series of the

densities (in amagat) of the gases. For the pure gas at a density ρ_a, the integrated absorption coefficient of the band can be written in the form

$$\int\alpha(\nu)d\nu = \alpha_{1a}\rho_a^2 + \alpha_{2a}\rho_a^3 + \ldots\ldots \quad . \tag{A-4}$$

For a binary mixture, the enhancement of the integrated absorption coefficient by the addition of a perturbing gas with a partial density ρ_b to the pure gas in the cell at a density ρ_a is expressed in the form

$$\int\alpha_{en}(\nu)d\nu = \alpha_{1b}\rho_a\rho_b + \alpha_{2b}\rho_a\rho_b^2 + \ldots\ldots \quad . \tag{A-5}$$

In eqs. (A-4) and (A-5), α_{1a} or α_{1b} (cm^{-2} $amagat^{-2}$) is the binary absorption coefficient and α_{2a} or α_{2b} (cm^{-2} $amagat^{-3}$) is the ternary absorption coefficient. The integrated absorption coefficients can be expressed in the following forms which are more convenient for comparison with the theory. For the pure gas

$$c\int\tilde{\alpha}(\nu)d\nu = \tilde{\alpha}_{1a}\rho_a^2 n_o^2 + \tilde{\alpha}_{2a}\rho_a^3 n_o^3 + \ldots\ldots \tag{A-6}$$

and for binary mixtures

$$c\int\tilde{\alpha}_{en}(\nu)d\nu = \tilde{\alpha}_{1b}\rho_a\rho_b n_o^2 + \tilde{\alpha}_{2b}\rho_a\rho_b^2 n_o^3 + \ldots\ldots \quad . \tag{A-7}$$

Here c is the speed of light, $\tilde{\alpha}(\nu)$ (= $\alpha(\nu)/\nu$) and $\tilde{\alpha}_{en}(\nu)$ (= $\alpha_{en}(\nu)/\nu$) are the coefficients of absorption and its enhancement at a frequency with the frequency factor removed, and n_o (= N_A/V_o) is Loschmidt's number (= 2.687×10^{19} cm^{-3}, number of molecules of an ideal gas per unit volume at S.T.P.). The new binary absorption coefficients $\tilde{\alpha}_{1a}$ and

$\tilde{\alpha}_{1b}$ represent transition probabilities induced in collisions of types a-a and a-b, respectively, and the new ternary coefficients $\tilde{\alpha}_{2a}$ and $\tilde{\alpha}_{2b}$ represent the transition probabilities induced in collisions of types a-a-a and a-b-b, respectively. The experimental absorption coefficients (cm^{-2} amagat^{-2} or cm^{-2} amagat^{-3}) are related to the new absorption coefficients ($cm^6\ s^{-1}$ or $cm^9\ s^{-1}$) as follows:

(A-8)
$$\tilde{\alpha}_{1a} = (c/n_o^2)\ \alpha_{1a}/\bar{\nu}\ ; \qquad \tilde{\alpha}_{1b} = (c/n_o^2)\ \alpha_{1b}/\bar{\nu}\ ,$$

$$\tilde{\alpha}_{2a} = (c/n_o^3)\ \alpha_{2a}/\bar{\nu}\ ; \qquad \tilde{\alpha}_{2b} = (c/n_o^3)\ \alpha_{2b}/\bar{\nu}\ .$$

Here $\bar{\nu}$, the centre of the band, is represented by

(A-9)
$$\bar{\nu} = \int\alpha(\nu)d\nu/\int\alpha(\nu)\nu^{-1}d\nu \qquad \text{(for the pure gas)}$$

or

$$\bar{\nu} = \int\alpha_{en}(\nu)d\nu/\int\alpha_{en}(\nu)\nu^{-1}d\nu \qquad \text{(for a binary mixture)}.$$

It can be shown (see, for example, Poll 1960)

(A-10)
$$\int\tilde{\alpha}(\nu)d\nu = \sum_{m<n} B_{mn}\, hc\, \frac{1}{V}\,(P_m - P_n) = \frac{8\pi^3}{3h}\,\frac{1}{V}\sum_{m<n}(P_m - P_n)|R^{mn}|^2$$

where B_{mn} ($= (8\pi^3/3h^2c)|R^{nm}|^2$) is the Einstein transition probability of absorption and m is the lower state and n is the upper state. P_m and P_n are the normalized Boltzmann factors giving the probabilities of finding the system in states m and n. The term with P_m corresponds to absorption and the term with P_n to stimulated emission. The summation $\sum_{m<n}$ indicates a sum over all pairs of states m and n for which $E_m < E_n$.

For the vibrational bands the term with P_n corresponding to stimulated emission may be neglected. Then eq. (A-10) reduces to

$$\int \tilde{\alpha}(\nu)d\nu = \frac{8\pi^3}{3h} \sum_m N_m |R^{nm}|^2 \qquad \text{(A-11)}$$

where N_m (= P_m/V) is the normalized number of molecules per cm^3 in the initial state m. The matrix elements R^{nm} of the electronic dipole moment are given by

$$R^{nm} = \int \psi_n^* M \psi_m d\tau \quad . \qquad \text{(A-12)}$$

For an isolated symmetric diatomic molecule in its ground electronic state, the electric dipole moment M is zero and, therefore, its infrared spectrum is ordinarily forbidden. However, if we consider collisions of such a molecule either with a similar symmetric diatomic molecule or some other foreign gas molecule, induced dipole moment occurs in the colliding pair. R^{nm} may then be represented as

$$R^{nm} = \langle v_1 v_2 J_1 J_2 | M | v_1' v_2' J_1' J_2' \rangle \qquad \text{(A-13)}$$

where v and J denote the vibrational and rotational states, respectively, and suffixes 1 and 2 represent molecules 1 and 2, respectively, of the colliding pair. For the fundamental band of molecule 1

$$R^{nm} = \langle 10\ J_1 J_2 | M | 00\ J_1' J_2' \rangle \quad . \qquad \text{(A-14)}$$

If the induced dipole moment M is expanded as Taylor's series in terms of the internuclear separations r_1 and r_2 and the vibrational wave functions of molecule 1 are separated, the matrix element can be written as

(A-15) $$R^{nm} = \langle 1|r_1 - r_0|0 \rangle \langle J_1 J_2|(\frac{\partial M}{\partial r_1})_0|J_1' J_2' \rangle \quad .$$

For a harmonic oscillator of reduced mass m_0 and frequency $\nu_0(s^{-1})$

(A-16) $$\langle 1|r_1 - r_0|0 \rangle = \kappa_1 = (h/8\pi^2 m_0 \nu_0)^{\frac{1}{2}} \quad .$$

Therefore,

(A-17) $$R^{nm} = \kappa_1 \langle (\frac{\partial M}{\partial r_1})_0 \rangle \quad .$$

In this expression, the matrix element corresponds to all single transitions in molecule 1 and double transitions in which molecule 1 makes the vibrational transition only and molecule 2 makes the rotational transition only.

Making use of eqs. (A-7), (A-11) and (A-17) and taking into account the translational motion of the colliding pair of molecules, Van Kranendonk (1957) represented the binary absorption coefficient of a specific rotational branch B of the collision-induced fundamental band of molecule 1 as

(A-18) $$\tilde{\alpha}_1(B) = \kappa \Sigma^{(B)} P_1 P_2 \int |M_1(\omega_1 \omega_2; R_{12})|^2 g_0(R_{12}) dR_{12} \quad .$$

Here $\kappa = \pi/3m_0\nu_0$ $(= (8\pi^3/3h)\kappa_1^2)$, P_1 and P_2 are the normalized Boltzmann factors for the initial states of molecules 1 and 2, respectively, $M_1(\omega_1\omega_2; R_{12}) = \langle J_1 J_2|(\frac{\partial M}{\partial r_1})_0|J_1' J_2' \rangle$ is the matrix element of the derivative of the induced dipole moment with respect to internuclear distance at the equilibrium position, $\omega_1 = (\theta_1, \phi_1)$ and $\omega_2 = (\theta_2, \phi_2)$ are the angles of the internuclear axes of molecules 1 and 2 relative to a

coordinate frame XYZ with its Z-axis lying along the vector R_{12} connecting the centre of mass of molecules 1 and 2, and $g_o(R_{12})$ is the pair distribution function. The quantity M_1 can be expanded in terms of spherical harmonics:

$$(A\text{-}19) \qquad \vec{M}_1(\omega_1\omega_2; \vec{R}_{12}) = 4\pi \sum_{\lambda_1\mu_1\lambda_2\mu_2} \vec{D}(\lambda_1\mu_1\lambda_2\mu_2; \vec{R}_{12})\, Y^{\mu_1}_{\lambda_1}(\omega_1)\, Y^{\mu_2}_{\lambda_2}(\omega_2) \quad .$$

For symmetric diatomic molecules the expansion coefficients $\vec{D}$ do not vanish only for even values of λ_1 and λ_2 and when $\mu_1 + \mu_2 = 0$ (Van Kranendonk 1951a). Van Kranendonk (1958) introduced an 'exp-4' model for the induced moment and used 'Lennard-Jones (6-12)' model for the intermolecular potential. According to the 'exp-4' model, the induced dipole moment consists of two parts: the long-range moment,which is angle-dependent,results from the polarization of one molecule by the quadrupole field of the other and is proportional to R^{-4}, R being the intermolecular separation; the short-range moment is due to the charge deformation induced by the electron overlap forces and decreases exponentially with increasing R. In this model the short-range moment is assumed to be spherically symmetric and its dependence on the mutual orientation of colliding pairs of molecules is neglected in the first approximation. The components $D\mu$ of the expansion coefficients $\vec{D}$ in (A-19) in the same coordinate frame are characteristic of the pair of colliding molecules. For possible values 1, 0 and -1 for μ, these components are given by

$$(A\text{-}20) \qquad D_{\pm 1} = \frac{1}{\sqrt{2}} (D_x + iD_y); \qquad D_o = D_z \quad .$$

The 'exp-4' model for the induced moment implies that the components of the expansion coefficients $\vec{D}$ in eq. (A-19) are assumed to have the following values:

(A-21)
$$D_0(0000) = \xi \exp(-R/\rho)$$

$$D_0(2000) = (3/\sqrt{5})\, Q_1' \alpha_2 / R^4$$

$$D_{\pm 1}(2 \pm 100) = (3/\sqrt{15})\, Q_1' \alpha_2 / R^4$$

$$D_0(0020) = -(3/\sqrt{5})\, \alpha_1' Q_2 / R^4$$

$$D_{\pm 1}(002 \pm 1) = -(3/\sqrt{15})\, \alpha_1' Q_2 / R^4 \quad .$$

Here Q_1 and α_1 are respectively the quadrupole moment and polarizability of molecule 1, the single prime indicates the first derivative with respect to the internuclear distance at the equilibrium position, and Q_2 and α_2 are respectively the quadrupole moment and polarizability of molecule 2.

When (A-19) is substituted into (A-18), the following expression results for the binary absorption coefficient of a specific rotational branch:

(A-22)
$$\tilde{\alpha}_1(B) = \kappa \sum_{\lambda_1 \lambda_2} L_{\lambda_1 \lambda_2}(B)\, I_0(\lambda_1 \lambda_2)$$

where

(A-23)
$$L_{\lambda_1 \lambda_2}(B) = \Sigma^{(B)}\, P(J_1)\, P(J_2)\, L_{\lambda_1}(J_1, J_1')\, L_{\lambda_2}(J_2, J_2')$$

and

$$I_o(\lambda_1\lambda_2) = \int \sum_{\mu_1\mu_2} |D(\lambda_1\mu_1\lambda_2\mu_2;\, R_{12})|^2\, g_o(R_{12})\, dR_{12} \tag{A-24}$$

where $\Sigma^{(B)}$ is sum over all the rotational quantum numbers J_1, J_2, J_1' and J_2' for which the transitions $J_1, J_2 \rightarrow J_1', J_2'$ contribute to the branch B, and P(J) are the normalized Boltzmann factors. The Racah coefficients L(J,J') are defined by

$$L_2(J,J')\, \delta_{\lambda\lambda'}\delta_{\mu\mu'} = 4\pi \sum_{mm'} \langle Jm|\lambda\mu J'm' \rangle \langle \lambda'\mu' J'm'|Jm \rangle \tag{A-25}$$

where

$$\langle Jm|\lambda\mu J'm' \rangle = \langle \lambda\mu J'm'|Jm \rangle^*$$

$$= \int Y_J^m(\omega)^*\, Y_\lambda^\mu(\omega)\, Y_{J'}^{m'}(\omega) d\omega \quad .$$

The Racah coefficients must satisfy the condition

$$\sum_{J'} L_\lambda(J,J') = 2J + 1 \tag{A-26}$$

so that the normalization condition for P(J) is written as

$$\sum_{J=0}^{\infty} (2J + 1)P(J) = 1 \quad . \tag{A-27}$$

For different rotational states of the ground vibrational level, P(J) are given by

$$P(J) = \frac{g_T \exp[-\, J(J + 1)B_o\, hc/kT]}{\sum_J (2J + 1)g_T \exp[-\, J(J + 1)B_o\, hc/kT]} \tag{A-28}$$

where $g_T = (2T + 1)$ is the degeneracy of the total nuclear spin T of the molecule. For hydrogen, T = 0 and 1.

The values of $L_\lambda(J,J')$ for $\lambda = 0$ and 2 are

(A-29)
$$L_0(J,J) = 2J + 1$$

$$L_2(J,J-2) = \frac{3(J-1)J}{2(2J-1)}$$

$$L_2(J,J) = \frac{J(J+1)(2J+1)}{(2J+1)(2J+3)}$$

$$L_2(J,J+2) = \frac{3(J+1)(J+2)}{2(2J+3)} \quad .$$

Substitution of (A-21) into (A-24) gives the non-vanishing integral

(A-30)
$$\kappa\, I_0(00) = \lambda^2\, \mathbf{I}\, \tilde{\gamma}$$

$$\kappa\, I_0(20) = \mu_1^2\, \mathbf{J}\, \tilde{\gamma}$$

$$\kappa\, I_0(02) = \mu_2^2\, \mathbf{J}\, \tilde{\gamma} \quad .$$

The dimensionless parameters λ, μ_1 and μ_2 are defined as

(A-31)
$$\lambda = (\xi/e)\, e^{-\sigma/\rho} \quad ;$$

$$\mu_1 = Q_1' \alpha_2 / e\sigma^4 \quad ;$$

$$\mu_2 = \alpha_1' Q_2 / e\sigma^4$$

where σ is the intermolecular distance R for which the intermolecular potential is zero, and e is the absolute value of the electronic charge. The significance of λ is that λe is the amplitude of the oscillating overlap dipole moment when the molecules are a distance σ apart and

μ_1^e and μ_2^e have similar meaning, and $\tilde{\gamma}$ is defined by

$$\text{(A-32)} \qquad \tilde{\gamma} = \frac{\pi e^2 \sigma^3}{3 m_0 \nu_0}$$

where m_0 and ν_0 are the reduced mass and the frequency of the molecular oscillation. The radial distribution integrals I and J are defined as

$$\text{(A-33)} \qquad I = 4\pi \int_0^\infty \exp(-2(x-1)\sigma/\rho) g_0(x) x^2 dx ,$$

$$\text{(A-34)} \qquad J = 12\pi \int_0^\infty x^{-8} g_0(x) x^2 dx ,$$

where $x = R^* = R/\sigma$ and $g_0(x)$ is the low density limit of the pair distribution function which is defined at high temperatures as

$$\text{(A-35)} \qquad g_0(x) = \exp\{-\phi(x)/kT\} ,$$

Here the intermolecular potential $\phi(x)$ is assumed to be the 'Lennard-Jones 6-12' potential ($\phi(x) = 4\epsilon(x^{-12} - x^{-6})$). At intermediate temperatures, $g_0(x)$ may be expanded in an asymptotic series in the powers of Planck's constant (de Boer 1949) in terms of the reduced temperature T^* ($= kT/\epsilon$) and the reduced mean de Broglie wavelength Λ^* ($= (h^2/m_{00}\,\epsilon\sigma^2)^{1/2}$) ($m_{00}$ being the reduced mass of the colliding pair of molecules). $g_0(x)$ can then be expressed as

$$\text{(A-36)} \qquad g_0(x) = \exp(-\phi^*(x)/T^*)\left\{1 + \frac{\Lambda^{*2}\sigma^2}{T^*\epsilon} W_2(x,T^*) + \frac{\Lambda^{*4}\sigma^4}{T^{*2}\epsilon^2} W_4(x,T^*) + \cdots\right\}$$

where

(A-37) $$W_2(x,T^*) = \frac{\epsilon}{48\pi^2\sigma^2}\left[\frac{\partial^2\phi^*(x)}{\partial x^2} - \frac{1}{2T^*}\left(\frac{\partial\phi^*(x)}{\partial x}\right)^2\right] , \quad \text{etc.}$$

Substituting eq. (A-36) into eqs. (A-33) and (A-34), we obtain

(A-38) $$\mathbf{I} = \mathbf{I}_{cl} - \Lambda^{*2}\ \mathbf{I}^{(2)} + \Lambda^{*4}\ \mathbf{I}^{(4)} + \ldots..$$

(A-39) $$\mathbf{J} = \mathbf{J}_{cl} - \Lambda^{*2}\ \mathbf{J}^{(2)} + \Lambda^{*4}\ \mathbf{J}^{(4)} + \ldots..$$

where

(A-40) $$\mathbf{I}_{cl} = 4\pi \int_0^\infty \exp(-2(x-1)\sigma/\rho)\exp(-\phi^*(x)/T^*)x^2dx$$

(A-41) $$\mathbf{I}^{(2)} = 4\pi \int_0^\infty \exp(-2(x-1)\sigma/\rho)\frac{\exp(-\phi^*(x)/T^*)}{T^*\epsilon/\sigma^2}W_2(x,T^*)x^2dx , \quad \text{etc.}$$

On substitution of (A-23 and (A-30), the expression (A-22) becomes

(A-42) $$\tilde{\alpha}_1(B) = [\lambda^2\,\mathbf{I}\,L_{oo}(B) + \mu_1^2\,\mathbf{J}\,L_{20}(B) + \mu_2^2\,\mathbf{J}\,L_{02}(B)]\tilde{\gamma} \quad .$$

The binary absorption coefficients of the individual lines with rotational quantum number J of the O ($\Delta J = -2$), Q ($\Delta J = 0$) and S ($\Delta J = 2$) branches of the induced fundamental band are expressed as follows:
For the pure gas

(A-43) $$\tilde{\alpha}_{1a}(O(J)) = (\mu_1^2 + \mu_2^2)\,\mathbf{J}\,\tilde{\gamma}\,P(J)\,L_2(J,J-2) \quad ,$$

(A-44) $$\tilde{\alpha}_{1a}(Q(J)) = \lambda^2\,\mathbf{I}\,\tilde{\gamma}\,P(J)\,L_0(J,J) + \mu_1^2\,\mathbf{J}\,\tilde{\gamma}\,P(J)\,L_2(J,J) + \mu_2^2\,\mathbf{J}\,\tilde{\gamma}\,P(J)\,\Sigma_{J'}P(J')\,L_2(J',J') \quad ,$$

and

(A-45) $$\tilde{\alpha}_{1b}(S(J)) = (\mu_1^2 + \mu_2^2)\, \mathbf{J}\, \tilde{\gamma}\, P(J)\, L_2(J,J+2) \quad .$$

For the binary mixtures

(A-46) $$\tilde{\alpha}_{1b}(O(J)) = \mu_1^2\, \mathbf{J}\, \tilde{\gamma}\, P(J)\, L_2(J,J-2) \quad ,$$

(A-47) $$\tilde{\alpha}_{1b}(Q(J)) = (\lambda^2\, \mathbf{I} + \mu_2^2\, \mathbf{J})\tilde{\gamma}\, P(J)\, L_0(J,J) + \mu_1^2\, \mathbf{J}\, \tilde{\gamma}\, P(J)\, L_2(J,J) \quad ,$$

and

(A-48) $$\tilde{\alpha}_{1b}(S(J)) = \mu_1^2\, \mathbf{J}\, \tilde{\gamma}\, P(J)\, L_2(J,J+2) \quad .$$

The total binary absorption coefficients $\tilde{\alpha}_{1a}$ and $\tilde{\alpha}_{1b}$ for the fundamental band are obtained by adding, after summation over J, eqs. (A-43), (A-44) and (A-45) for the pure gas and eqs. (A-46), (A-47) and (A-48) for a binary mixture. By doing so, a single expression results for both cases, which can be expressed as

(A-49) $$\tilde{\alpha}_{1a} \text{ or } \tilde{\alpha}_{1b} = \lambda^2\, \mathbf{I}\, \tilde{\gamma} + (\mu_1^2 + \mu_2^2)\, \mathbf{J}\, \tilde{\gamma} \quad .$$

Here $\lambda^2\, \mathbf{I}\, \tilde{\gamma}$ is the overlap part and $(\mu_1^2 + \mu_2^2)\, \mathbf{J}\, \tilde{\gamma}$ is the quadrupolar part. When the perturbing molecule b is monatomic, Q_2 equals 0 and hence $\mu_2 = 0$. Eq. (A-48) then reduces to

(A-50) $$\tilde{\alpha}_{1b} = \lambda^2\, \mathbf{I}\, \tilde{\gamma} + \mu_1^2\, \mathbf{J}\, \tilde{\gamma} \quad .$$

Recent calculations of Karl and Poll (1967) have shown that Q' of molecular hydrogen is sensitive to the values of J and J'. Therefore, eq. (A-50) can only be simplified into

$$\text{(A-51)} \qquad \tilde{\alpha}_{1b} = \lambda^2 \mathbf{I}\,\tilde{\gamma} + \mathbf{J}\,\tilde{\gamma} \sum_J P(J)\,[\mu_1^2(J,J-2)\,L_2(J,J-2) + \mu_1^2(J,J)\,L_2(J,J) + \mu_1^2(J,J+2)\,L_2(J,J+2)]$$

where $\mu_1(J,J') = \dfrac{Q_1'(J,J')\alpha_2}{e\sigma^4}$. A method of calculation of $Q_1'(J,J')$ will be described in Appendix B.

The occurrence of the dip in the Q branch of the collision-induced fundamental bands has been explained recently by Van Kranendonk (1968) on the basis of an interference effect due to correlations existing between the short-range overlap dipole momentsin successive collisions.

APPENDIX B

MATRIX ELEMENTS OF THE QUADRUPOLE MOMENT OF H_2

The molecular quadrupole moment for fixed nuclei in units of ea_0^2, referred to a coordinate system with the Z-axis along the internuclear axis of a diatomic molecule, is given by

$$Q(r) = \frac{1}{2} r^2 - \langle 3z_1^2 - r_1^2 \rangle \tag{B-1}$$

where r is the internuclear distance of the molecule and z_1 and r_1 are the Z-coordinate and radius vector, respectively, of one of the electrons. In (B-1) the first term on the right-hand side corresponds to the contribution from the nuclei and the second term with angular brackets to the contribution from the electrons to the quadrupole moment. The angular brackets denote the expectation value over the ground electronic state. The radial matrix elements of the quadrupolar moment, referred to the fixed frame of the molecule, between two states having radial wave functions ψ_{vJ} and $\psi_{v'J'}$ normalized with respect to dr are

$$\langle vJ \mid Q \mid v'J' \rangle = \int \psi^*_{vJ}(r)\, Q(r) \psi_{v'J'}(r) dr \quad . \tag{B-2}$$

Here the wave functions ψ_{vJ} are solutions of the Schroedinger wave equation for the relative nuclear motion:

$$\frac{d^2\psi_{vJ}(r)}{dr^2} + \left[\frac{4\pi\,\mu c}{\hbar}\{E - U(r)\} - \frac{J(J+1)}{r^2}\right] \psi_{vJ}(r) = 0 \quad . \tag{B-3}$$

The adiabatic values of the matrix elements of the quadrupole moment of H_2, HD and D_2 have been evaluated by numerical integration of (B-2) for the pure rotational transitions and for the 1-0, 2-0, 3-0, 4-0 and 5-0 bands by Karl and Poll (1967) and Birnbaum and Poll (1969). The functions ψ_{vJ} in (B-2) in the adiabatic approximation (i.e. by using the adiabatic potential for the ground electronic state neglecting the influence of the excited electronic states) are obtained by these authors by numerical integration of (B-3) (for details, see Karl and Poll 1966) using the effective potential U(r) of H_2 from the work of Kolos and Wolniewicz (1964, 1965, 1968). The function of Q(r) of H_2 in (B-2) is taken from the data of Kolos and Wolniewicz (1965).

Karl and Poll (1967) outlined a method which is useful as a partial check on the numerical calculations mentioned above. In this method they treated the effect of the rotation-vibration interaction on the matrix elements by the perturbation theory. They expanded the radial wave functions ψ_{vJ} with J = 0 in terms of the 'unperturbed' functions ψ_{vo}. They represented the correction $\Delta Q(vJ|v'J')$ to the matrix elements due to rotation-vibration interaction by the relation

$$(B\text{-}4) \qquad \langle vJ \mid Q \mid v'J' \rangle = \langle v0 \mid Q \mid v'0 \rangle + \Delta Q(vJ|v'J') \quad .$$

In the first order perturbation theory

$$(B\text{-}5) \qquad \Delta Q(vJ|v'J') = - \sum_{v_1 \neq v} \frac{\langle v'0 \mid Q \mid v_1 0 \rangle \langle v_1 0 \mid \dot{y} \mid v0 \rangle}{E_{v_1 o} - E_{vo}} - \sum_{v_2 \neq v'} \frac{\langle v0 \mid Q \mid v_2 0 \rangle \langle v_2 0 \mid \dot{y}' \mid v'0 \rangle}{E_{v_2 o} - E_{v'o}}$$

where the perturbations V and V' (rotational energies in ergs) are given by

$$(B\text{-}6) \qquad V = J(J+1)\,\hbar^2/2\mu r^2 \;, \quad V' = J'(J'+1)\,\hbar^2/2\mu r^2 \;.$$

When the matrix elements of $Q(r)$ and r^{-2} in the harmonic-oscillator approximation are close to the actual values (i.e. in the cases of $\Delta v = 0$ and 1), the functions can be approximated into harmonic-oscillator wavefunctions. $Q(r)$ and $V(r)$ are then expanded in powers of $(r - r_e)$ up to the second order:

$$(B\text{-}7) \qquad Q(r) = Q_0 + Q_1(r - r_e) + Q_2(r - r_e)^2$$

$$V(r) = BJ(J+1)\left[1 - \{2(r - r_e)/r_e\} + \{3(r - r_e)^2/r_e^2\}\right]$$

where $B = \hbar^2/2\mu r_e^2$, and the constants Q_0, Q_1 and Q_2 are obtained by means of a least square fit of $Q(r)$ in (B-7) to the data for H_2 given by Kolos and Wolniewicz (1965). Therefore, the relative matrix elements in the harmonic-oscillator approximation are

$$(B\text{-}8) \qquad \langle v \mid Q \mid v \rangle = Q_0 + Q_2 r_e^2\,(B/\omega)(2v+1) \;,$$

$$\langle v \mid Q \mid v+1 \rangle = Q_1 r_e\,(B/\omega)^{\frac{1}{2}}(v+1)^{\frac{1}{2}} \;,$$

$$\langle v \mid Q \mid v+2 \rangle = Q_2 r_e^2\,(B/\omega)(v+1)^{\frac{1}{2}}(v+2)^{\frac{1}{2}} \;,$$

$$\langle v \mid V \mid v+1 \rangle = -2BJ(J+1)(B/\omega)^{\frac{1}{2}}(v+1)^{\frac{1}{2}} \;,$$

$$\langle v \mid V \mid v+2 \rangle = 3BJ(J+1)(B/\omega)(v+1)^{\frac{1}{2}}(v+2)^{\frac{1}{2}} \;,$$

and similarly for ψ'. Substituting eq. (B-8) into eq. (B-5) finally we have

$$\Delta Q(vJ \mid v+1\ J') = [J(J+1) - J'(J'+1)]\ 2Q_0(B/\omega)^{3/2}(v+1)^{\frac{1}{2}}. \tag{B-9}$$

Using $B = 60.9\ cm^{-1}$, $\omega = 4162\ cm^{-1}$ and $Q_0 = 0.457\ ea_0^2$ for H_2, Karl and Poll (1967) have shown that the calculated correction term $\Delta Q(0J|1J')$ by means of (B-9) are consistent with the corresponding differences of the numerically-evaluated matrix elements of the quadrupole moment.

The matrix elements $< 0J \mid Q \mid 1J' >$ of the Q and S branches evaluated numerically for H_2 by Birnbaum and Poll (1969) are listed in Table B-1. The values calculated by us for the O(2) and O(3) lines of H_2 with the help of (B-4) and (B-9) are also included in the same table.

TABLE B-1

MATRIX ELEMENTS FOR THE FUNDAMENTAL BAND OF HYDROGEN IN UNITS OF ea_0^2

J	O-branch	Q-branch	S-branch
	$< 0J \mid Q \mid 1\ J-2 >$	$< 0J \mid Q \mid 1J >$	$< 0J \mid Q \mid 1\ J+2 >$
0		0.08793*	0.07835*
1		0.08800*	0.07206*
2	0.09764	0.08815*	0.06586*
3	0.10411	0.08836*	0.05974*

*Values calculated by Birnbaum and Poll (1969).

ACKNOWLEDGMENTS

The author wishes to express his grateful thanks to his research supervisor, Dr. S. P. Reddy, for his valuable guidance and advice through all phases of the research work leading to the present thesis.

The author's thanks are due to Professor S. W. Breckon, Head of the Department of Physics, for his continued interest in this research. Thanks are also due to Professor C. W. Cho and Dr. G. Varghese for useful discussions. Grateful acknowledgments are also due to several faculty members of the Department of Physics, from whom the author has learned much through lectures and discussions.

The financial support received from Memorial University of Newfoundland and from Dr. Reddy's N.R.C. operating grant A-2440 in the form of fellowships is gratefully acknowledged.

The author appreciates the use of computer facilities and the assistance of the staff of Technical Services. He is also thankful to the staff of the machine shop of the Department of Physics for their assistance throughout the progress of the experiments.

REFERENCES

1. American Institute of Physics Handbook, 1963.
2. Benedict, W. S. and Plyler, E. K., 1951. J. Res. Natl. Bur. Stds. 46, 246.
3. Birnbaum, A. and Poll, J. D., 1969. Private communication.
4. Bishop, R. B., 1966. M.Sc. Thesis, Memorial University of Newfoundland.
5. De Boer, J., 1949. Repts. Progr. Phys. 12, 305.
6. Britton, F. R. and Crawford, M. F., 1958. Can. J. Phys. 36, 761.
7. Chisholm, D. A. and Welsh, H. L., 1954. Can. J. Phys. 32, 291.
8. Condon, E. V., 1932. Phys. Rev. 41, 759.
9. Crawford, M. F., Welsh, H. L., and Locke, J. L., 1949. Phys. Rev. 75, 1607.
10. Dean, J. W., 1961. Natl. Bur. Stds. Technical Note 120.
11. Gush, H. P., Nanassy, A., and Welsh, H. L. 1957. Can. J. Phys. 35, 712.
12. Hare, W. F. and Welsh, H. L., 1958. Can. J. Phys. 36, 88.
13. Hirschfelder, J. O., Curtiss, C. F., and Bird, R. B., 1967. Molecular Theory of Gases and Liquids, 2nd Edition (Wiley, New York).
14. Humphreys, C. J., 1953. J. Opt. Soc. Am. 43, 1027.
15. Hunt, J. L., 1959. Ph.D. Thesis, University of Toronto.
16. Hunt, J. L. and Welsh, H. L., 1964. Can. J. Phys. 42, 873.
17. Karl, G. and Poll, J. D., 1967. J. Chem. Phys. 46, 2944.
18. Kuo, C. Z., 1970. M.Sc. Thesis, Memorial University of Newfoundland.
19. Mann, D. B., 1962. Natl. Bur. Stds. Technical Note 154.
20. Michels, A., De Graaff, W., Wassenaar, T., Levelt, J. M. H., and Louwerse, P., 1959. Physica 25, 25.

21. Michels, A. and Wouters, H., 1941. Physica 8, 923.

22. Michels, A., Wassenaar, T., and Louwerse, P., 1960. Physica 26, 539.

23. Perkin-Elmer Instruction Manual, Vol. 1, Vol. 3A.

24. Plyler, E. K., Blaine, L. R., and Tidwell, E. D., 1955. J. Res. Natl. Bur. Stds. 55, 279.

25. Plyler, E. K., Blaine, L. R., and Nowak, M. J., 1957. J. Res. Natl. Bur. Stds. 58, 195.

26. Poll, J. D., 1960. Ph.D. Thesis, University of Toronto.

27. Poll, J. D. and Karl, G., 1966. Can. J. Phys. 44, 1467.

28. Reddy, S. P. and Cho, C. W., 1965. Can. J. Phys. 43, 793.

29. Reddy, S. P. and Cho, C. W., 1965. Can. J. Phys. 43, 2331.

30. Reddy, S. P. and Lee, W. F., 1968. Can. J. Phys. 46, 1373.

31. Sears, V. F., 1968a. Can. J. Phys. 46, 1163.

32. Sears, V. F., 1968b. Can. J. Phys. 46, 2315.

33. Sinha, B. B. P., 1967. M.Sc. Thesis, Memorial University of Newfoundland.

34. Stoicheff, B. P., 1957. Can. J. Phys. 35, 730.

35. I.U.P.A.C. Table of Wavenumbers for the Calibration of Infrared Spectrometers, 1961 (Butterworths, London).

36. Timmerhaus, K. D., 1963. Advancesin Cryogenic Engineering (Plenum Press, New York), Vol. 8, 135.

37. Van Kranendonk, J. and Bird, R. B., 1951a. Physica 17, 953.

38. Van Kranendonk, J. and Bird, R. B., 1951b. Physica 17, 968.

39. Van Kranendonk, J., 1957. Physica 23, 825.

40. Van Kranendonk, J., 1958. Physica 24, 347.

41. Van Kranendonk, J. and Kiss, Z. J., 1959. Can. J. Phys. 37, 1187.

42. Van Kranendonk, J., 1968. Can. J. Phys. 46, 1173.

43. Varghese, G. and Reddy, S. P., 1969. Can. J. Phys. 47, 2745.

44. Watanabe, A. and Welsh, H. L., 1964. Phys. Rev. Letters 13, 810.

45. Watanabe, A. and Welsh, H. L., 1965. Can. J. Phys. 43, 818.

46. Watanabe, A. and Welsh, H. L., 1967. Can. J. Phys. 45, 2859.